JYVÄSKYLÄ STUDIES IN COMPUTING
211

Hannu-Heikki Puupponen

Unmixing Methods in Novel Applications of Spectral Imaging

JYVÄSKYLÄN YLIOPISTO

JYVÄSKYLÄ STUDIES IN COMPUTING 211

Hannu-Heikki Puupponen

Unmixing Methods in Novel Applications of Spectral Imaging

Esitetään Jyväskylän yliopiston informaatioteknologian tiedekunnan suostumuksella
julkisesti tarkastettavaksi yliopiston Agora-rakennuksen Beeta-salissa
joulukuun 19. päivänä 2014 kello 12.

Academic dissertation to be publicly discussed, by permission of
the Faculty of Information Technology of the University of Jyväskylä,
in building Agora, Beeta hall, on December 19, 2014 at 12 o'clock noon.

UNIVERSITY OF JYVÄSKYLÄ

JYVÄSKYLÄ 2014

Unmixing Methods in Novel Applications of Spectral Imaging

JYVÄSKYLÄ STUDIES IN COMPUTING 211

Hannu-Heikki Puupponen

Unmixing Methods in Novel Applications of Spectral Imaging

UNIVERSITY OF JYVÄSKYLÄ

JYVÄSKYLÄ 2014

Editors
Timo Männikkö
Department of Mathematical Information Technology, University of Jyväskylä
Pekka Olsbo, Ville Korkiakangas
Publishing Unit, University Library of Jyväskylä

URN:ISBN:978-951-39-6016-2
ISBN 978-951-39-6016-2 (PDF)

ISBN 978-951-39-6015-5 (nid.)
ISSN 1456-5390

Jyväskylä University Printing House, Jyväskylä 2014

ABSTRACT

Puupponen, Hannu-Heikki
Unmixing Methods in Novel Applications of Spectral Imaging
Jyväskylä: University of Jyväskylä, 2014, 38 p.(+included articles)
(Jyväskylä Studies in Computing
ISSN 1456-5390; 211)
ISBN 978-951-39-6015-5 (nid.)
ISBN 978-951-39-6016-2 (PDF)
Finnish summary
Diss.

Application areas of hyperspectral imaging have expanded tremendously during the last decade with the improved availability of high-resolution spectral cameras and less expensive, more compact high-speed computing machinery with which to process the resulting datasets. These developments have resulted in great potential in the use of more advanced algorithms and methods for processing and visualizing spectral data to derive new information concerning wide variety of targets and objects in such varied fields of application as environmental monitoring, security, forensics and medicine. The articles included contain some of the results of the studies the author has contributed to in each of these fields. The overall focus is on the utilization of spectral unmixing methods for deriving new, useful and valuable information from the subjects examined. This both opens up avenues for further research, and potential for marketable products based on new spectral sensors and for utilization of spectral unmixing as one step in data processing and analysis.

Keywords: hyperspectral imaging, spectral unmixing, target detection, imaging spectrometry, forensics, environmental monitoring, skin abnormalities

Author

Hannu-Heikki Puupponen
Department of Mathematical Information Technology
University of Jyväskylä
Finland

Supervisor

Pekka Neittaanmäki
Department of Mathematical Information Technology
University of Jyväskylä
Finland

Reviewers

Professor Maria Skopina
Saint Petersburg State University
Russia

Docent Veikko Hara
University of Jyväskylä
Finland

Opponent

Docent Tuomo Kauranne
Lappeenranta University of Technology
Finland

ACKNOWLEDGEMENTS

> Some tricks of the light you'll never know,
> make a flickering midnight light into a
> glow.
>
> Mike Oldfield - Tricks of the Light

Many persons have contributed to these studies and to my overall academic career, and I extend my thanks to all who have collaborated with me, either in actual research and its contents, or in discussions, by providing encouragement and support.

I thank in particular the supervisor of this work, Prof. Pekka Neittaanmäki, and the reviewers, Docent Veikko Hara and Prof. Maria Skopina. Their comments and encouragement were indispensable for the success of this process. I am grateful for Ph.D. Steve Legrand for checking my use of the English language.

I extend my gratitude to the co-authors and co-workers in the research projects that led to this dissertation, in no particular order: Ilkka Pölönen, Jaana Kuula, Tapani Reinikainen, Tapani Kalenius, Heikki Saari, Heikki Rinta, Marko Haukkamäki, Tuomas Teräväinen, Johanna Salmelin, Tuomas Selander, Heikki Hämäläinen, Anna Karjalainen, Ari Väisänen, Kari-Matti Vuori, Ismo Pellikka, Eija Honkavaara, Antti Lindfors, Lauri Markelin, Teemu Hakala, Kimmo Nurminen, Noora Neittaanmäki-Perttu and Mari Grönroos. Their contributions and efforts were invaluable and of high scientific integrity.

I would like to mention several former and current colleagues who have supported me and provided both encouragement and ideas in the course of my career this far, again in no particular order: Jani Puttonen, Kari Aho, Osmo Schroderus, Olli Alanen, Janne Kurjenniemi, Ilmari Repo, Markku Lauttamus, Petri Räisänen, Juhana Keskinen, Onni Kyrö, Erkki Kurkinen, Kauko Keränen, Vesa Arkko, Antti Juvonen, Tuomo Sipola, Tapani Ristaniemi, Tero Tuovinen, Jouko Nieminen, Eetu Rantakangas, Markku Häkkinen, Pertti Hakkarainen, Heikki Salo and all members of MST team.

My family has always been there for me, and has provided both guidance and strength to proceed further in my academic pursuits and life. I thank all the current and departed members of my extended family: Tuula Valkama-Puupponen, Hannu Puupponen, Veli-Mikko Puupponen, Lulu, Hilla, Pippa, Tia, Dixi, Viljo, Väinö and Venla. I especially thank Radium, Ferdinand, Sigma and Friedrich.

Edited and typeset on Sun Microsystems SPARCStation 10.

ACRONYMS

CBRNE	Chemical, Biological, Radiological, Nuclear and Explosive
FVA	Filter Vector Algorithm
ICA	Independent Component Analysis
MNF	Minimum Noise Fraction
NNLS	Non-Negative Least Squares
PCA	Principal Component Analysis
PGP	Prism-Grating-Prism
PPI	Pixel Purity Index
SGA	Simplex Growing Algorithm
SNR	Signal-to-Noise Ratio
SVD	Singular Value Decomposition
SWIR	Shortwave Infrared
UAV	Unmanned Aerial Vehicle
VCA	Vertex Component Analysis

LIST OF FIGURES

LIST OF ALGORITHMS

CONTENTS

LIST OF INCLUDED ARTICLES

PI Jaana Kuula, Ilkka Pölönen, **Hannu-Heikki Puupponen**, Tuomas Selander, Tapani Reinikainen, Tapani Kalenius and Heikki Saari. Using VIS/NIR and IR spectral cameras for detecting and separating crime scene details. *Proceedings of SPIE Vol. 8359, Sensors, and Command, Control, Communications and Intelligence (C3I) Technologies for Homeland Security and Homeland Defense XI, 83590P (May 1, 2012); doi:10.1117/12.918555;*, 2012.

PII Jaana Kuula, **Hannu-Heikki Puupponen**, Heikki Rinta, Ilkka Pölönen. The challenges of analysing blood stains with hyperspectral imaging. *Proc. SPIE 9112, Sensing Technologies for Global Health, Military Medicine, and Environmental Monitoring IV, 91120W (5 June 2014); doi: 10.1117/12.2050180*, 2014.

PIII Jaana Kuula, **Hannu-Heikki Puupponen**, Heikki Rinta, Ilkka Pölönen, Marko Haukkamäki, Tuomas Teräväinen. Detecting explosive substances by the IR spectrography. *Proc. SPIE 9073, Chemical, Biological, Radiological, Nuclear, and Explosives (CBRNE) Sensing XV, 90730Q (10 June 2014); doi: 10.1117/12.2050157*, 2014.

PIV Johanna Salmelin, Ilkka Pölönen, **Hannu-Heikki Puupponen**, Heikki Hämäläinen, Anna Karjalainen, Ari Väisänen, Kari-Matti Vuori. Hyperspectral imaging of benthic macroinvertebrates - a novel tool for detecting metal contamination in running waters. *Manuscript. To be submitted.*, 2014.

PV Ilkka Pölönen, **Hannu-Heikki Puupponen**, Eija Honkavaara, Antti Lindfors, Heikki Saari, Lauri Markelin, Teemu Hakala, Kimmo Nurminen. UAV-based hyperspectral monitoring of small freshwater area. *Proc. SPIE 9239, Remote Sensing for Agriculture, Ecosystems, and Hydrology XVI, 923912 (10 October 2014); doi: 10.1117/12.2067422*, 2014.

PVI **Hannu-Heikki Puupponen**, Ilkka Pölönen, Noora Neittaanmäki-Perttu, Pekka Neittaanmäki, Mari Grönroos, Heikki Saari. Spectral unmixing for the separation of Lentigo Maligna and Lentigo Maligna Melanoma. *Submitted to Medical Engineering and Physics, Elsevier*, 2014.

Hyperspectral imaging is a multidisciplinary field combining the needs for expertise in imaging, computation, spectrometry and such target research areas as forensics, environmental sciences and medicine. This has led the author to work in several research groups and projects involving experts from all these fields. The author acted in these projects mainly in roles related to specification of experiments and instruments, performing the experiments and execution of data analysis.

Articles [PI]-[PIII] originating from the SpeCSI project, examine potential applications of hyperspectral imaging and data analysis for forensic science, and

with a particular focus on rapid investigation directly at the scene of the crime. The author was involved in designing the experimental setups, and analyzing and interpreting the collected data. This created the basis for further studies into development of instruments, procedures and software to be utilized in the field of forensic work.

Papers [PIV] and [PV] concern environmental monitoring, and originate from the author's involvement in the Zoobenthos-ICT and HSI-Stereo projects. For paper [PIV] the author participated in experiment design and execution and in planning the data analysis. Paper [PV] involved the author in results interpretation and planning for further studies.

Article [PVI] results from a long-term project to improve diagnostics of potentially malicious skin abnormalities. Also here the author was involved in the design of the instrument, performing imaging on the patients and designing the data analysis. A related patent has been applied for, and the method shows considerable promise for rapidly determining the borders of skin abnormalities for more effective surgical excision and improved treatment response.

1 INTRODUCTION

1.1 Background

Color and reflectivity in general as an inherent property of objects was conceptualized early in the study of vision and optics. Roger Bacon described in his Opus Majus how rays of light and color reflected from an object and entering the eye are the enabling agent of vision [Bacon, 1267]. Spectrally selective absorption was first described by William Hyde Wollaston in 1802. He utilized a prism to observe spectra from different light sources, discovering 'distinct dark lines' in the solar spectrum and further noting that light from a candle or an electric light gives rise to sets of spectral features differing from the ones he found in sunlight [Wollaston, 1802]. These direct observational results would be fully explained during the 19th century through work of Fraunhofer, Bunsen, Kirchhoff and others as resulting from each distinct substance having a dissimilar ability to absorb, and conversely reflect or emit, different wavelengths of electromagnetic radiation, one frequency range of which is visible light.

A precedent to multispectral imaging methods could be considered to have presented itself in the color-separation technique of color photography. It was first proposed in [Maxwell, 1857] and afterwards demonstrated in 1861 by James Clerk Maxwell: three regular black and white photography plates were exposed in sequence through colored filters to respectively capture red, green and blue light. By projecting the three plates simultaneously with correct registration through the same three color filters, a rendition of the image in full color would result. Following development of panchromatic photographic materials, this method enabled vivid reproduction of color, as for example displayed by Sergey Prokudin-Gorsky in his famed series of color photographs documenting the Russian Empire.

From these historical beginnings of spectroscopy and imaging color analysis the field of spectral imaging proper came into its own through the use of multispectral sensors in various mapping and surveillance satellites in 1960s and 1970s, for example the well-known Landsat series of satellites [Williams et al., 2006].

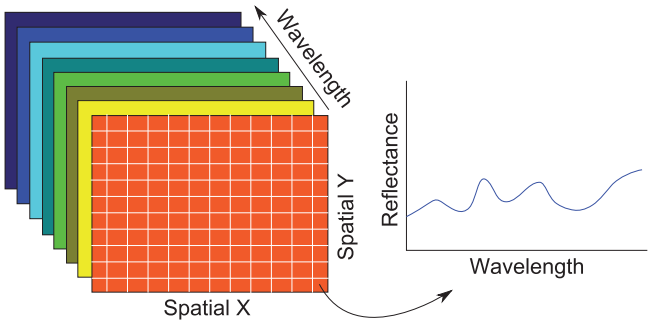

FIGURE 1 Generic structure of a hyperspectral datacube

Simultaneously with these developments radical improvements in computing machinery enabling efficient processing of the resulting large data sets has made it possible for application of spectral imaging to emerge as a multi-disciplinary, exploratory field of research with wide-ranging possibilities for practical applications and with novel ways to examine and observe both new and already known phenomena.

The difference between multispectral and hyperspectral sensors is typically defined primarily by the relative narrowness of the wavelength bands at which the individual intensity measurements are captured and secondarily by the number of these wavebands, with hyperspectral sensors often reaching at least one hundred or considerably more wavebands. The resulting hyperspectral dataset, usually termed a datacube, contains an intensity image plane acquired at each distinct waveband, thus providing each pixel with associated spectral information. This spectral definition enables a more precise analysis for separating and indentifying objects, substances and targets from the image data. In hyperspectral imaging spatial information plays a lesser role, as the improved spectral resolution in the dataset allows more knowledge to be derived from the spectral analysis [Chang, 2013]. This is what sets it apart from being simply an extended mode of multispectral imaging. The generic structure of a hyperspectral datacube is illustrated in Figure 1.

There are several technical approaches for implementing the acquisition of a spectral datacube in practice. The main criteria between divisions of device classes range from the direction the acquisition process traverses the datacube to the specific technical means the spectral separation is achieved. From a directional viewpoint, instruments can be divided into ones that capture the complete spectral data simultaneously either for one image-plane pixel or one image-plane line while traversing the spatial dimension during capture of a complete scene and into those that capture one image plane at a time, traversing the spectral dimension of the datacube during image capture. For spectral separation several technical approaches have emerged, including filter wheels, different types of interferometers, dispersive elements like prisms or gratings and acousto-optical and liquid-crystal tunable filters [Chang, 2007].

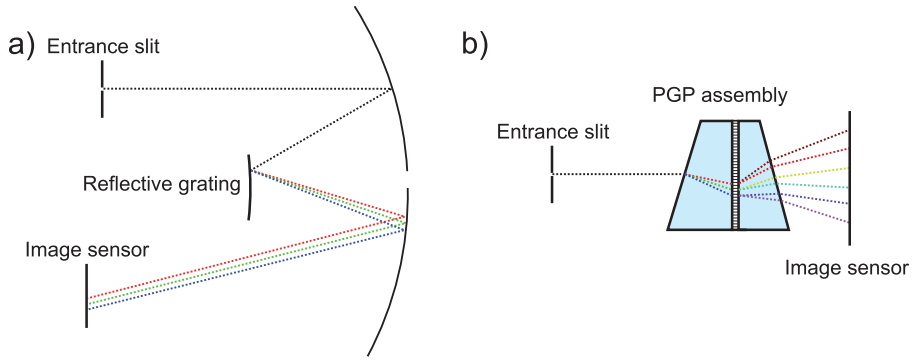

FIGURE 2 Spectrograph principles used for push broom imagers: a) an Offner-type spectrograph utilizing reflective grating to achieve spectral separation; b) the functional principle of a Prism-Grating-Prism (PGP) spectrograph.

Imagers that capture complete spectral information and have some means to traverse the spatial dimension are conventionally termed whisk broom and push broom imagers, respectively proceeding one image-plane pixel or one image-plane line at a time. These devices typically display advantages in terms of good signal-to-noise ratio and relatively quick data acquisition. A potential challenge is the requirement for a beam-steering solution, a linear scanner or a rotation platform to achieve full-scene coverage. Applications where the subject is inherently in motion, as for example in many industrial processes or on a sufficiently stable flight platform moving over terrain, are especially suitable for this type of device, since in these cases the specific disadvantageous requirement is negated.

One common method to implement a push broom device is through some type of a spectrograph to disperse the incoming image plane line onto a two-dimensional image sensor, thus directly achieving complete spectral information from that line. Two examples of commercially utilized principles are the Offner spectrograph and the prism-grating-prism (PGP) construction. The former has been commercialized by Headwall Photonics, and while providing excellent performance figures, the design needs to accommodate for the angled optical path, increasing difficulties when constructing compact equipment. The latter is utilized by Specim and has the advantage of a straight optical path and relative compactness with it.[Aikio, 2001] These two spectrograph designs are illustrated in Figure 2.

Imagers that operate one image plane at a time, traversing the spectral dimension of the data cube, are usually termed frame imagers or staring instruments. One of their advantages is the possibility to potentially realize a more compact device, as no equipment to enable spatial scanning is required. Another upside is the possibility to adapt, to the specific application, the amount of data captured, as only relevant wavebands can usually be acquired under the program control, thus minimizing the capture time, data transmission, storage and processing requirements. Downsides include often poorer noise performance re-

sulting from the light-transmission properties of their tunable filter or interferometer arrangements and relatively long capture times for complete, spectrally contiguous datacubes creating additional challenges with changing scenes or objects in motion.

Hyperspectral datasets are, in several ways, demanding to process. There is a relatively large amount of data, considering that instead of one image with three intensity values for each pixel as in case of a normal RGB color image, potentially several hundred values of intensity information are associated with each image-plane pixel. From this also follows the high-dimensional nature of the spectral datacubes, requiring advanced processing and visualization methodologies to extract and present actionable knowledge. Additionally, very often in real world scenes, many of the pixels receive reflections from more than one material present, either directly mixed together or occurring within the same pixel, due to the pixel covering a target area greater than the one covered only by the specific substance or object. To be able to distinguish and quantify these mixed spectral traces, we need spectral mixture analysis, the main research method utilized in this work.

1.2 Research Approach

The concept of spectral unmixing can be divided between approaches that model the mixing process in a linear and those that accomplish this in nonlinear fashion. In this study, we mostly concern ourselves with the linear variety of methods. Spectral unmixing generally defines an inverse problem, namely, we have a dataset of mixed pixels potentially containing spectral information from several different materials or objects, and we need to find out their extent and proportion. To solve this problem, it is necessary to devise a model of the mixing process for forming an inverse process determining the individual contributing spectra and their proportions. These idealized classes of spectral components are typically termed endmembers [Chang, 2007].

The linear mixture model is based on the assumption that the target displays a checkerboard-like separation between materials, with single reflections of the illuminating radiation from each impinging on a sensor element. This model was first formulated in remote sensing context in [Horwitz et al., 1971]. In linear mixture modeling, the complete spectrum arriving at each detector pixel is described as a linear combination of the constituent endmember spectra. If we have M endmembers, whose spectra are $S = [s_1 s_2 \cdots s_M]$ and their fractional abundances $a = [a_1 a_2 \cdots a_M]^T$, it is possible to express the spectrum of a mixed pixel x as $x = \sum_{k=1}^{M} a_k s_k + w = Sa + w$, where w is a noise term, including error factors like sensor noise and mixing-model imperfections.

The contrasting nonlinear models assume an intimate mixture of materials giving rise to multiple, scattering reflections from each constituent material,

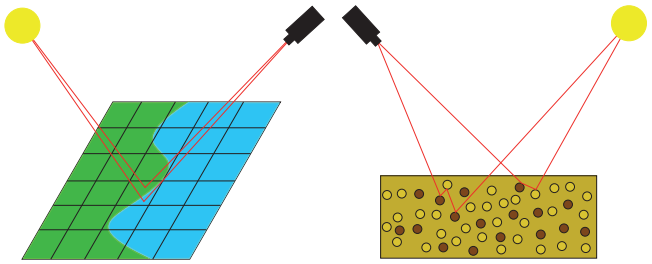

FIGURE 3 Examples of linear and nonlinear mixing model assumptions. On the left, in case of macroscopic mixing, rays reflected just once arrive from each material to the sensor resolution element. In the nonlinear case on the right, within a single sensor pixel, there is an intimate mixture of materials with multiple reflections and scattering.

consequently requiring a more involved nonlinear model to account for the aggregate spectrum arriving at the detector pixel [Keshava, 2003]. Nonlinear mixing models often are specific to a given set of conditions or types of target substances, or utilize computationally expensive numerical methods. These properties increase the desirability of utilizing the linear mixing assumption where practicable. The scenarios representing the two spectral mixture models are illustrated in Figure 3. The approach in this study is to utilize the linear mixing model and examine how usable it is in novel real world applications, which are closer to a field study scenario than laboratory environment or synthetic test data, and see what useful information and actionable knowledge can be derived in each of these application fields. The applications examined are in the areas of forensic science, environmental monitoring and clinical medicine, providing a wide variety of different requirements and target materials.

The research question considered in this study can thus be formulated to address an inquiry concerning whether linear mixing model and spectral mixture analysis derived from this modeling assumption are able to provide useful additional knowledge in real world applications. This is examined through verifying the viability with target area knowledge and with experts of environmental monitoring, forensics and medical diagnostics. This brings an additional viewpoint in each publication concerning the value and usability of the methodology for each of the application areas and specific studies detailed in the included publications.

1.3 Structure of the Work

After describing the general background and the specific research approach in the first chapter, the second chapter further defines the methods utilized. In the third chapter, the applications studied in the included papers are described and, in the fourth, the results are shortly described with conclusions drawn on the overall

research direction taken and on the possibilities and avenues that are open for further studies.

1.4 Related Publications and Presentations

Utilizing knowledge discovery model for databases as a framework for the spectral data analysis, Ilkka Pölönen approached some of the same applications in his dissertation [Pölönen, 2013]. The focus of his work is on processing data captured by a prototype Fabry-Perot interferometer-based hyperspectral imager, as described in [Saari et al., 2009]. Earlier results in the fields of forensics and skin diagnostics are described and evaluated in his work, while the other main applications are agri- and silvicultural remote sensing with the compact hyperspectral instrument installed on an unmanned aerial vehicle. In contrast, this dissertation considers any hyperspectral imaging device and more general applicability of linear spectral mixture analysis for the examined fields of study.

Presentations including the author's contribution on the crime scene and security applications of hyperspectral imaging and spectral mixture analysis have been given in a conference dealing with defense against CBRNE threats [Kuula et al., 2012, 2] and in another one dealing with forensic science [Kuula et al., 2012, 1]. These representations were well received in the respective conferences and generated further interest in the potential of hyperspectral data analysis in these application fields.

2 METHODOLOGY

2.1 Overall Steps of Spectral Unmixing

The overall process of determining the constituent material spectra and establishing their relative proportions in the scene imaged takes place in practically three separate steps, for each of which different methods and underlying assumptions can be chosen. The first of these steps, after any instrument-related, radiometric and atmospheric corrections and possible cropping have been applied to the data, is dimensionality reduction. This step is not strictly necessary: some endmember induction methods operate without it, but it often can provide a compaction of the data, thus reducing the memory footprint and computational requirements [Keshava, 2003]. The second step is endmember induction, which generates an estimation of the distinct constituent spectra of which the mixed pixels in the scene consist of. Finally, the third step, inversion, generates abundance maps, a set of image planes that indicate the fractional abundances of the extracted endmembers in each pixel.

For this general framework of a typical spectral unmixing process, many different methods can be chosen for each of the steps, shown in Figure 4. In the following subsections, several methods for each step of the process are shortly described and compared.

2.1.1 Dimensionality Reduction

Dimensionality reduction in general seeks to retain most of the information content of the data while reducing the high-dimensional hyperspectral dataset into a less computationally demanding volume of data and providing potential SNR improvements. There are several possible approaches based on statistical assumptions and properties of the spectral dataset. The classical second order statistics of principal component analysis or maximum noise fraction are some of the possibilities, but often the sample set in hyperspectral data for many less common spectral features is insufficient to be effectively presented by these meth-

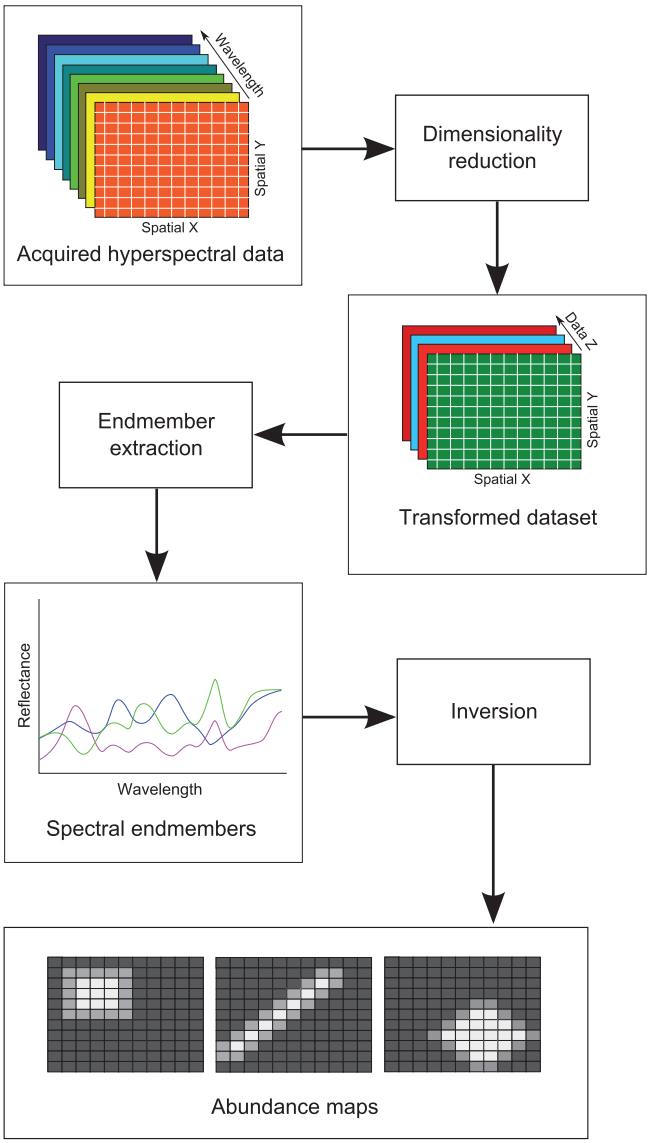

FIGURE 4 Steps of the utilized spectral data analysis process.

ods [Chang, 2013]. These two methods, respectively, order data components by maximum data variance and by maximum signal to noise ratio. Due to this, MNF can be viewed as a noise-adjusted version of PCA [Lee et al., 1990].

Another method for dimensionality reduction is the utilization of traditional singular value decomposition to present the data matrix, practically describing the data components ordered in terms of maximum power. We can reduce the dimensionality by zeroing out the components with the least energy represented, thus retaining most of the information content while reducing the size and, therefore, computational complexity of the data set. Further methods can utilize other higher-order statistical properties like skewness, kurtosis and statistical independence of the data components [Chang, 2013]. In this work, most-used dimensionality reduction methods are PCA and SVD; the endmember extraction methods employed are able to use also other dimensionality reduction approaches; and one avenue for further study would be to examine what advantages the use of for example ICA or any non-linear, stochastic method for dimensionality reduction might provide in these applications.

2.1.2 Endmember Induction

The next step of the spectral unmixing process is to estimate a set of endmembers explaining the mixed pixels in the data. Endmember extraction algorithms can be broadly separated into two classes, depending on whether all endmembers are generated at the same time in a single step or by sequentially expanding the pool of endmembers as the extraction proceeds onwards [Chang, 2013]. These general approaches have different advantages. Simultaneous extraction practically amounts to an exhaustive search and comes with the associated high computational cost. Sequential extraction can be less than optimal: the starting conditions and the way the sequence is formed can lead to a less pure set of endmembers compared to the complete exhaustive search for candidates, but sequential selection can in turn greatly reduce the required computational effort.

The two best-known simultaneous endmember extraction algorithms are the pixel purity index (PPI) and N-FINDR. PPI was first presented in [Boardman, 1994], and is based on generating random unit vectors, often termed skewers, and projecting the data onto these vectors. The projection is then examined to form a set of data points ending up on the extremities of this projection. The more often a data point finds itself at an extremity as all random projection vectors are examined, the higher the purity index it will attain, and thus it will end up being more likely as an endmember selection. PPI with two skewers is illustrated in Figure 5. A non-iterative PPI algorithm is presented as Algorithm 1. A downside to this method is that to function effectively at discovering endmembers, a high number of skewers is required, leading to a high computational cost as a large pool of random vectors is generated and investigated. Another disadvantage is that the method is not very stable, randomly generated projection sets resulting in potentially different endmember sets with each run [Chaudry et al., 2006].

N-FINDR approaches the same problem in a different manner, by itera-

Algorithm 1 Pixel Purity Index

$N \leftarrow$ number of skewers
$x \leftarrow$ all datapoints
$y \leftarrow$ zero matrix to hold the PPI counts
$d \leftarrow$ number of elements in x
$t \leftarrow$ threshold index for considering a point an endmember
$i \leftarrow 0$
for $i \leq N$ **do**
    $s \leftarrow$ random unit vector with dimensions of the datapoints
    $maxval \leftarrow 0$
    $minval \leftarrow 0$
    for all j **in** x **do**
        $val \leftarrow j \cdot s$
        if $val > maxval$ **then**
            $j_{max} \leftarrow j$
            $maxval \leftarrow val$
        else if $val < minval$ **then**
            $j_{min} \leftarrow j$
            $minval \leftarrow val$
        end if
    end for
    $y[j_{max}] \leftarrow y[j_{max}] + 1$
    $y[j_{min}] \leftarrow y[j_{min}] + 1$
    $i \leftarrow i + 1$
end for
for all k **in** y **do**
    if $k \geq t$ **then**
        k is added into the endmember set
    end if
end for

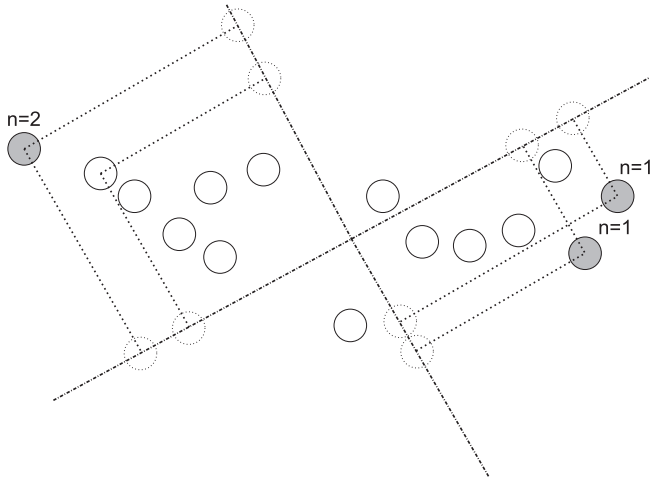

FIGURE 5 PPI with two skewers. To select between two points with one extremity each, additional skewers would be necessary.

tively searching for a larger simplex in the data rather than using random projections to estimate the extent. Initially, a random starting set of endmember candidates within the data are selected. Afterwards, for each candidate endmember, every image pixel is inspected, and should this pixel spectrum provide an increase in the simplex volume, it would replace the current endmember candidate. The algorithm proceeds in this manner repeatedly for all the endmember candidates until no more replacements are performed [Winter, 1999]. It is immediately clear that the computational cost will be considerable, as the algorithm amounts to a straightforward search for endmember candidates giving the highest simplex volume in the data. Depending on how the random initial candidates were positioned, many replacements could be performed. The original description given by Winter is open to interpretation as to the exact manner the iteration is performed and the endmember replacements performed. Additionally, more specific methods can be used for selecting the initial endmember candidates. These permutations for the N-FINDR concept are discussed for example in [Plaza et al., 2005] and [Chang, 2013].

Two representative examples of sequential methods are the vertex component analysis and simplex growing algorithm. Of these, VCA was presented in [Nascimento et al., 2005] and operates by repeatedly performing orthogonal subspace projections, using previously discovered endmembers as spanning vectors for this subspace. The algorithm then finds the extreme of this projection, which is added as the next endmember, until the desired number of endmembers have been generated. The algorithm thus operates by using the earlier convex hull to generate a new one better conforming to the data simplex. This methodology of extrema selection by sequential projection makes VCA comparable to a sequential version of PPI, which is also noted in [Chang, 2013]. Owing to this much

reduced amount of projections and extremity inspections, VCA has one to two orders of magnitude lower computational cost than for example N-FINDR or PPI [Nascimento et al., 2005].

SGA in turn operates by first selecting a single random initial endmember within the data and starting to grow a simplex by adding the next data point so that of all points possible to be added to the n-vertex simplex the selected point $n+1$ gives the highest simplex volume. This process is illustrated in Figure 6. The algorithm proceeds in this manner until the required number of endmembers have been generated by iteratively adding new furthermost points into the simplex. A general outline of SGA is included as Algorithm 2. This is advantageous in terms of computational cost in comparison to N-FINDR, as we are now only adding a single new vertex each time, while N-FINDR, depending on the initial random conditions, is replacing vertices repeatedly [Chang et al., 2006]. As orthogonal projections are faster to perform than simplex volume calculations, VCA is one of the fastest endmember extraction algorithms, while SGA also performs considerably better than PPI or N-FINDR [Chang, 2013]. SGA can be considered to implement a sequential version of N-FINDR. There are also other means to sequentialize the simplex-finding process of N-FINDR, but SGA serves as the main representative for our general overview.

Algorithm 2 Simplex Growing Algorithm

$p \leftarrow$ number of endmembers to be extracted
$x \leftarrow$ all datapoints
$e_1 \leftarrow$ random datapoint from x
$i \leftarrow 1$
while i < p **do**
  $maxvol \leftarrow 0$
  x is reduced into i dimensions through a dimensionality reduction method
  for all j **in** x **do**
    $vol \leftarrow \dfrac{\left| det \begin{bmatrix} 1 & 1 & \cdots & 1 & 1 \\ e_1 & e_2 & \cdots & e_i & j \end{bmatrix} \right|}{i!}$
    if $vol > maxvol$ **then**
      $j_{max} \leftarrow j$
      $maxvol \leftarrow vol$
    end if
  end for
  $e_{i+1} \leftarrow j_{max}$
  $i \leftarrow i+1$
end while

An important concern for the performance of sequential endmember induction methods is correct specification of the number of endmembers to be generated. Sometimes it is possible to determine this information from a prior scene or application area knowledge, when it is known beforehand how many distinct

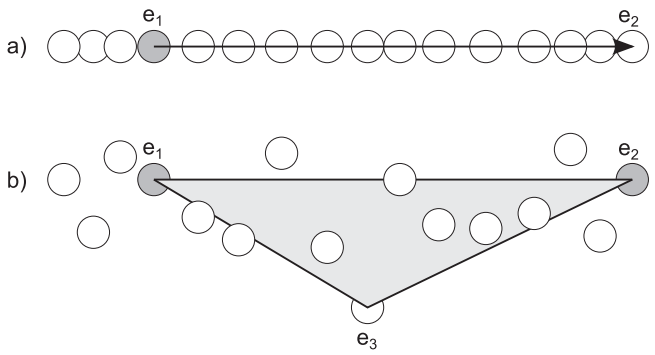

FIGURE 6 Progress of SGA from initial random endmember into the second one in a) and further to the third one in b), maximizing the distance and then the triangle area covered by selecting data points giving maximum simplex volume.

materials will be present in the scene or area of interest imaged. Another approach is to examine the properties of the data itself to determine the probable number of distinct endmembers the scene can be expected to hold. To this end, one can also use PCA-based methods, but weak sources of still distinct spectral signatures might not contribute enough energy to be detected by examining the eigenvalue distribution.

An approach based on examining the difference between sample matrix correlation and covariance eigenvalues has been suggested in [Harsanyi et al., 1993]. When formulating a Neyman-Pearson detector for determining between the hypothesis of the correlation and covariance eigenvalues being the same and the hypothesis of correlation eigenvalue being greater than the corresponding covariance eigenvalue, it becomes possible to determine whether an endmember is potentially contributing to the energy at the component, as for white noise the eigenvalues would be equivalent.

2.1.3 Inversion

The final step of the overall unmixing process, inversion, takes as inputs the endmember spectra estimated in the previous step and the original spectral datacube. The aim of the process is the generate abundance images, giving the fractional abundances of each endmember in each of the image pixels. This inverse problem can be solved in several ways, and to be physically realizable, the resulting fractional abundances need to fulfill two conditions. These are the additivity condition, which states that all abundances present a sum equal to unity, and the non-negativity condition, stating that no fractional abundance may be negative in value [Keshava, 2003]. The most common solution for the inversion problem in the field of spectral imaging is the different variations of the least squares method. Non-negative least squares is one usable variant, and satisfies the non-negativity condition [Lawson et al., 1974]. Numerically solving the least squares problem

for each image element is computationally expensive, especially as the number of endmembers increases.

Another approach to the inversion problem is the filter vector algorithm proposed by [Bowles et al., 1995]. This method is based on the classical signal processing technique of matched filtering. In this method, the filter vectors are selected to be orthogonal to endmember spectra other than the one the specific vector is matched for. This is carried out by generating a pseudo-inverse matrix $\mathbf{P}$ from $\mathbf{P} = \left(X^T X\right)^{-1} X^T$, where X is a columnar endmember matrix. Now the abundance fraction estimate $\hat{\alpha}$ for a given pixel spectrum Y can be obtained from $\hat{\alpha} = \mathbf{P}Y$. In this manner, the unconstrained variant of the inversion problem is reduced to once generating the pseudo-inverse matrix $\mathbf{P}$ and afterwards performing the multiplication for each image element Y, resulting in a low computational complexity. The trade-off for the computationally relatively fast method is that FVA fulfills neither of the constraints for physically realizable abundance fractions.

2.2 Example of Spectral Data Analysis

As an example of the process to perform spectral unmixing, a sample unmixing process with a trivial dataset is presented. This data has been chosen to easily demonstrate the process flow rather than any difficulty to unmix successfully. The test image displays corners of four squares on a X-Rite ColorChecker reference target. The image was acquired with a prototype Fabry-Perot interferometer-based hyperspectral camera, yielding 60 usable spectral bands from 503 nm to 818 nm at 320x240 image plane pixels. The image was cropped to exclude any border effects, and dark-point and illumination corrections were performed to yield reflectance values. A false-color rendition of the dataset is presented in Figure 7.

The first step with the data is the performance of dimensionality reduction. As our data has consistent colored areas, it should be easy to characterize. Examining the first two principal components already shows five clear clusters: a central one that contains the dark pixels on the divider and four deviating cluster containing the colored pixels. The first two principal components are displayed in Figure 8.

After dimensionality reduction, we are ready to perform endmember induction. Knowing that we have four colored squares in the image, we specify four endmembers to be extracted. A virtual dimensionality test for the data also estimates the four distinct spectral signatures. Utilizing VCA for endmember extraction, we get endmember spectra shown in Figure 9. The endmember spectra would appear to correspond well to the colors of the squares imaged, indicating a successful endmember extraction result.

The final step in the spectral mixture analysis is inversion, which yields abundance planes displaying the abundance of each endmember found in the image. Using FVA to give an inversion result, we find the colored squares corre-

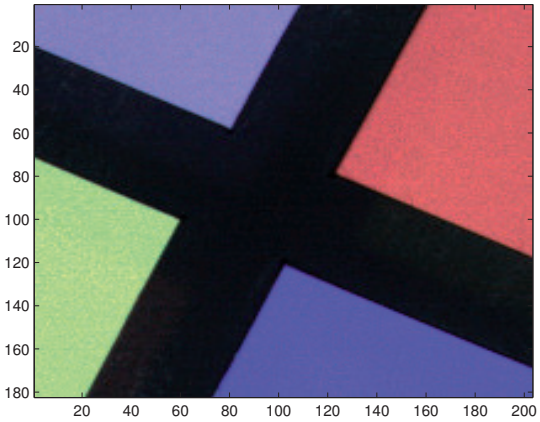

FIGURE 7 False-color rendition of the sample data, with one waveband from the datacube chosen to respectively present closely corresponding RGB colorplane.

sponding to each endmember spectra. This results in a clear distinction of each color from the dataset. The result is shown in the composite color image in Figure 10, where each color corresponds to one of the endmembers.

2.3 Methods Used in Studies

In the included papers, we utilized the dimensionality reduction scheme the standard implementation of VCA specifies. Depending on a SNR threshold, the VCA algorithm selects either a PCA- or SVD-based approach, this adaptation having been shown to offer improved noise performance [Nascimento et al., 2005]. For endmember extraction we consistently chose VCA, due to its very good computational performance and sufficient endmember induction capabilities. The computational complexity is of added importance in the clinical and field-oriented cases we studied. Similarly, this was a consideration when selecting the inversion algorithm, and in all cases where total processing time was of any importance, we utilized FVA. When the time taken for analysis was not an issue, NNLS was deployed. Generally, the differences between abundance estimates produced by FVA and NNLS were found to be minor for the applications studied, thus the savings in computational complexity afforded by the use of FVA were found well justified.

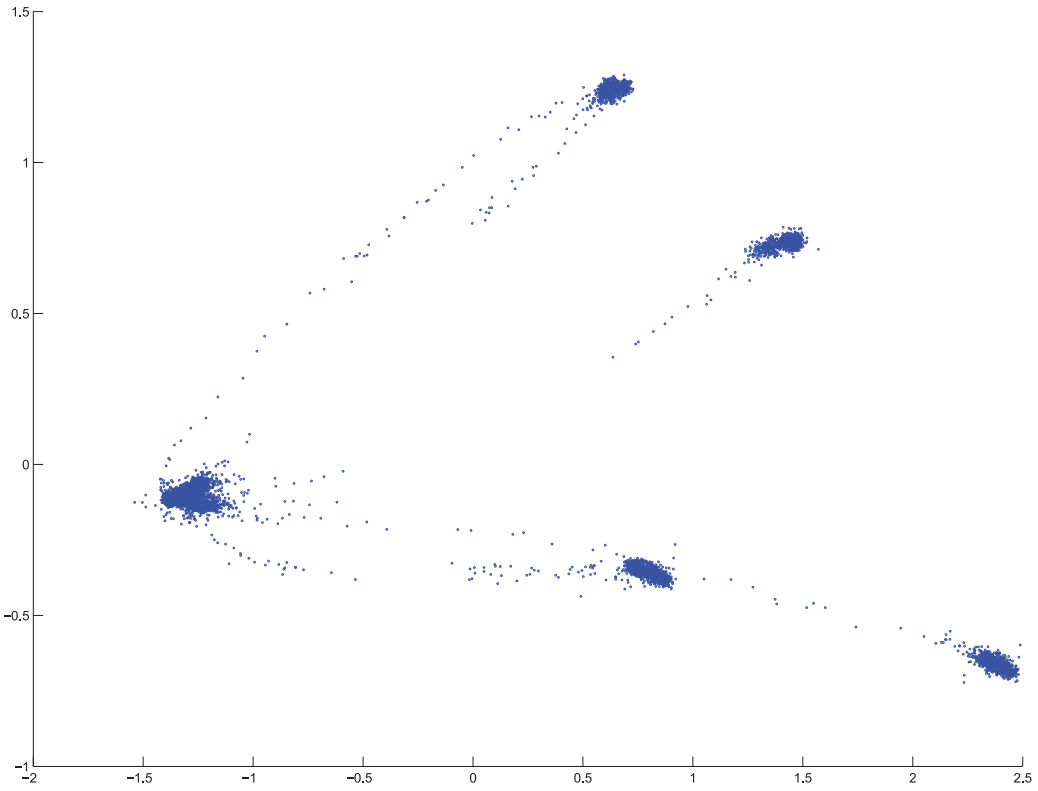

FIGURE 8 The first two principal components of the sample data, revealing a central cluster containing dark pixels and four outlying cluster containing colored pixels. The edges of the colored squares contain the few mixed pixels seen between the central cluster and the others.

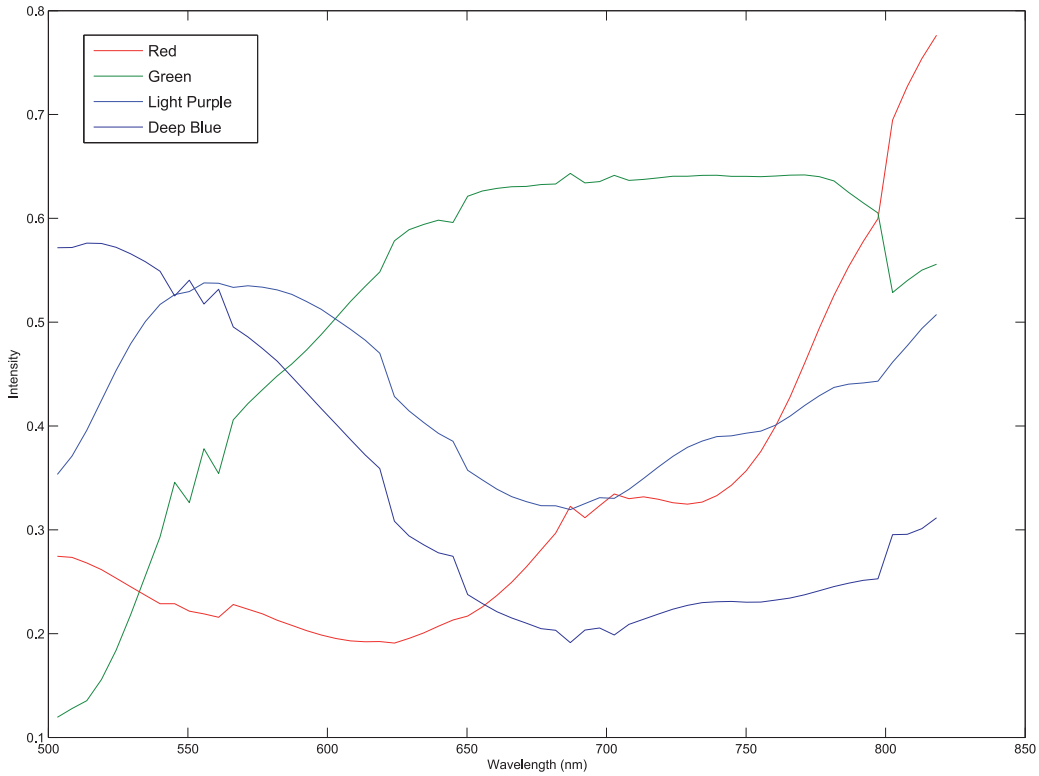

FIGURE 9 VCA-extracted endmember spectra, with a good correspondence to the respective colored squares present in the image.

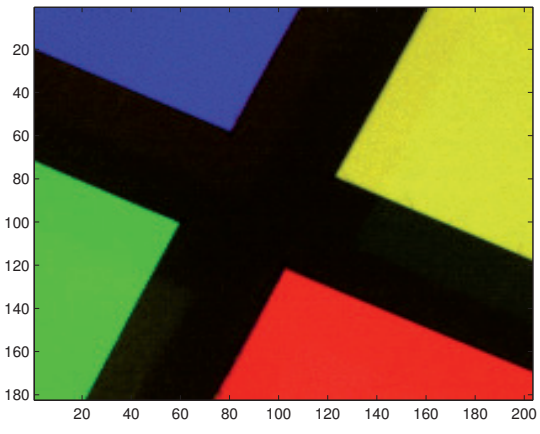

FIGURE 10 A color composite showing the abundances of each of the four endmembers, the colors corresponding to one endmember each.

3 RESULTS

In this chapter, we shortly examine the results in each field of study. [PI], [PII] and [PIII] are publications concerning forensics and crime scene investigation where spectral imaging and spectral unmixing are used. In [PIV] and [PV] spectral mixture analysis is utilized for monitoring the condition of aquatic environments, both through directly imaging the body of water with a UAV system and by examining an indicator species. Finally, a diagnostic application for skin abnormalities is described in [PVI].

3.1 Forensics

Separation and detection of traces and stains of forensic interest has been an important research topic, especially as ability to already roughly separate and classify trace evidence at the crime scene itself would both enable a faster investigation procedure at the scene of crime and lighten the load on laboratories examining the evidence gathered. Another important consideration is that, through being able to use spectral imaging to detect and classify traces, more evidence would remain completely intact for laboratory examination, as detection would not require chemical methods or handling the evidence.

With these advantages in mind, in [PI] an overall study was performed on the efficacy of spectral imaging and spectral unmixing methods at detecting and separating various types of traces typically found at the scene of a violent crime. Three different spectral imagers were utilized, and especially SWIR-range imager gave promising results with its separation of different paints and bloodstains originating from several donors. Additionally, for example untreated latent fingerprints and gunshot-originated primer residue were examined, but considering the modest resolution and magnification of the instruments utilized and the corresponding resolving power required for these targets, none of the instruments tested were able to detect these traces.

After the promising initial results, further studies were planned and per-

formed especially towards the separation of bloodstains. The results of these were presented in [PII]. It proved that separation of bloodstains through spectral features only is of more limited utility than the initial results would have led one think, as most of the properties of blood that characterize an individual are in concentrations and levels of detail far beyond the ability of typical hyperspectral cameras to detect. It is probable that the sample preparation and handling in the first study were not sufficiently rigorous, and, with increased precision in the further studies, the bloodstains proved much more difficult to separate. It is evident that a rough classification is possible, with properties like erythrocyte count and oxidation of the hemoglobin correlating with spectral features, but more specific analysis to determine individuals needs to be performed with traditional laboratory methods.

Rapid screening and stand-off detection of explosive substances and traces is of considerable importance both for pre-emptive security applications and for forensic work when explosive devices have been detonated. This was not examined in the original overview, after which series of experiments into this topic have been performed and are described in [PIII]. The results show that there is potential to detect explosive residues with the help of hyperspectral imaging, as long as the residue is directly visible and of sufficient amount and concentration to give a distinguishable signal. As the only application for a separate instrument, this might not be sufficient, but if the hyperspectral camera is used as a part of a multi-sensor array, or also simultaneously for other detection and screening applications, the potential ability to detect explosives and explosive traces is a highly useful addition.

3.2 Environmental Monitoring

Rapid monitoring of water quality, especially the methods giving positional information about eutrophication and pollution issues, is of considerable importance in monitoring sources of environmental degradation. Towards this end, two different studies were performed. The first one, described in [PIV], utilizes an indicator species to monitor the body of water against heavy metal pollution. The experiment and method utilized did provide a promising basis towards being able to use hyperspectral imaging as a faster, less labor-intensive method for screening the indicator species for heavy metal exposure. The current state of the art being microscopic examination of one specimen at a time, further study could present an important development for these types of environmental methods.

The second paper [PV] examines hyperspectral methods for directly monitoring a body of water from an UAV. This kind of approach would enable fast examination of large areas through the use of a lightweight hyperspectral imager on an UAV platform, monitoring the body of water for eutrophication by examining the amount of organic matter, chlorophyll and the overall turbidity of the water. The imaging nature of the method would also enable pinpointing localized

sources of nutrients or other water quality issues. This approach requires further study of the data captured, as the initial results utilize only a narrow wavelength range in comparison to the other datasets available, thus indicating potential for improved results with additional analysis.

3.3 Diagnostics of Skin Abnormalities

Diagnostics of potentially malignant skin abnormalities has been a research interest for several years, this far resulting in the development of a specialized imaging system for the application and in several publications on the topic. Current research progress in the topic is outlined in [PVI], which includes a short description of the technical imaging solution utilized and the analysis methods which are in line with the approach described in this introduction. The accuracy and applicability of the methodology has been verified through histopathological sampling and examination, and it has proven to be of utility in real clinical conditions. Going forward, this is an important result, which enables further study both towards applying the device and the methodology in a wider scale to skin diagnosis requirements and potentially creating an improved device viable for commercialization and further research.

This area holds considerable interest as more precise abnormality border demarcation could considerable improve the treatment response, both through reducing the need for re-excisions and reducing the chance that the issue would resurface. Especially surgical excision of actinic keratosis requires well-defined borders to ensure the best possible treatment results, as even a minor amount of affected cells remaining can lead to renewed occurrence of the keratosis later on. Against this background, a rapid, non-invasive method to better define the borders of the abnormality and potentially also distinguish between Lentigo Maligna and Lentigo Maligna Melanoma would offer an improvement upon the state of the art in clinical practice, which underlines the significance of this result.

4 CONCLUSION

In conclusion, the included papers display different levels of success with applying linear spectral mixture analysis to real world problems. Of these, [PVI] is especially promising, with verified results and usability in clinical practice. Further direction of interest in studies would be application of nonlinear mixture analysis based on modeling the inherently multi-layered structure of skin and critically comparing the results achieved against the currently outlined hyperspectral approach. This type of improvement in the data processing approach can also be deployed easily in the form of a software update if the imaging equipment is already in place.

The forensic investigations as lined out in [PI], [PII] and [PIII] are an area of moderate promise. In this application the main challenge is the field usage scenario for quickly screening an actual scene of crime. The area is bound to contain many types of materials, and separating the potentially physically small traces of interest from the scene requires either high magnification, slowing the screening process down, or very high spatial resolution, in turn increasing instrument cost and processing requirements considerably. Another challenge is the fact that it is naturally impossible through imaging detect traces that are not directly visible, concealed by other items, by furniture for example. In the near future a more probable usage scenario will consist of different laboratory devices extending the range of instruments and methods available to the central and field laboratories, but in the longer term more compact and affordable infrared hyperspectral cameras and improved sensor resolution might make this application viable for direct field application.

Further study is required, above all, in environmental monitoring applications, where the results are still inconclusive. In case of [PIV], the experiment setup, cadmium exposure arrangements and the interpretation of the tissue concentration results in relation to the data gathered by hyperspectral imaging need to be re-examined, as the current approach gives at best a tenuous correlation between the three parts of the experiment. This does not necessarily mean that the method would not hold potential, but the experiment as performed might not be sufficient to establish the facts either way. [PV] holds a different set of

challenges, considering the potentially too low SNR of the dataset and that linear mixture model might not be sufficient to describe this situation. Additionally, further study will include data captured at other sets of wavebands, as the one between 400 nm and 500 nm is not the most promising set when considering the library spectra used for comparison.

Overall the original research question about whether linear spectral mixture analysis is able to extract useful information and actionable knowledge in various novel applications of hyperspectral imaging has been positively answered in this study. Some of the applications require more further study than others or are less viable to be deployed currently due to other technical considerations but, in each, the linear methodology did prove useful. Linear unmixing provides an unsupervised and computationally fast generic method, which is a valuable tool for quickly analyzing a hyperspectral dataset, also before potentially applying or developing more complex, possibly application-specific analysis methods and approaches.

YHTEENVETO (FINNISH SUMMARY)

Hyperspektrikuvantaminen on alkanut laajentua uusiin käyttötarkoituksiin viime vuosien ja vuosikymmenten aikana, saatuaan alkunsa kaukokartoitusmenetelmistä ovat instrumenttien pienentyminen, edullisempi hinta ja laskentakapasiteetin saatavuuden paraneminen johtaneet sovellusalueiden ja analyysimenetelmien monipuolistumiseen. Tässä väitöskirjassa tarkastellaan kolmea uudehkoa spektrikuvantamisen ja spektrierottelumenetelmien käyttöalaa. Rikospaikkatutkinnan, ihomuutosten diagnostiikan ja ympäristötekniikan tarkastelluissa sovelluksissa pyritään hyödyntämään erityisesti lineaarista spektrierottelua osana analyysimenetelmää, ja osoittamaan laskennalliselta vaativuudeltaan nopean lineaarisen spektrierottelun olevan hyödyllinen, tai jopa osan sovelluksista kannalta riittävä toimenpide. Tutkimusten tulokset tukevat tätä väittämää, ja tarjoavat useita jatkotutkimuksen mahdollisuuksia.

REFERENCES

[Aikio, 2001] Aikio, M. 2001. *Hyperspectral Prism-Grating-Prism Imaging Spectrograph*. Technical Research Centre of Finland, VTT Publications 435.

[Bacon, 1267] Bacon, R. 1267. *Opus Majus*. Williams and Norgate. 1900

[Boardman, 1994] J.W. Boardman. 1994. *Geometric mixture analysis of imaging spectrometery data*. Proc. Int. Geoscience and Remote Sensing Symp. Vol. 4.

[Bowles et al., 1995] Bowles, J. H., Palmadesso, P. J., Antoniades, J. A., Baumback, M. M., Lee, J. 1995. *Use of Filter Vectors in Hyperspectral Data Analysis* Proc. SPIE 2553, Infrared Spaceborne Remote Sensing III

[Chang et al., 2006] Chang, C., Liu, W. 2006. *A New Growing Method for Simplex-Based Endmember Extraction Algorithm*. IEEE Transactions on Geoscience and Remote Sensing, Vol. 44, No. 10

[Chang, 2007] Chang, C. (ed.) 2007. *Hyperspectral Data Exploitation - Theory and Applications*. Wiley

[Chang, 2013] Chang, C. 2013. *Hyperspectral Data Processing*. Wiley

[Chaudry et al., 2006] Chaudry, F., Wu, C., Liu, W., Chang, C., Plaza, A. 2006. *Pixel purity index-based algorithms for endmember extraction from hyperspectral imagery* in Recent Advances in Hyperspectral Signal and Image Processing, 2006, Chang, C. (ed.), Transworld Research Network.

[Drake et al., 1999] Drake, N. A., Mackin, S., Settle, J. J. 1999. *Mapping Vegetation, Soils and Geology in Semiarid Shrublands Using Spectral Matching and Mixture Modeling of SWIR AVIRIS Imagery*. Remote Sens. Environ. 68. Elsevier

[Harsanyi et al., 1993] Harsanyi, J., Farrand, W., Chang, C. 1993. *Determining the number and identity of spectral endmembers: An integrated approach using Neyman.Pearson eigenthresholding and iterative constrained RMS error minimization*. Proc. 9th Thematic Conf. Geologic Remote Sensing.

[Horwitz et al., 1971] Horwitz, H. M., Napelka, R. F., Hyde, P. D., Morgenstern, J. P. 1971. *Estimating the Proportion of Objects within a Single Resolution Element of a Multispectral Scanner*. Proc. 7th International Symposium on Remote Sensing of Environment

[Keshava, 2003] Keshava N. *A Survey of Spectral Unmixing Algorithms*. Lincoln Laboratory Journal. Volume 14, Number 1. 2003.

[Kuula et al., 2012, 1] Kuula, J., Pölönen, I., Puupponen, H-H., Reinikainen, T., *The Challenge of Using Hyperspectral Imaging in Crime Scene Investigation*, EAFS2012 - Towards Forensic Science 2.0, The Hague.

[Kuula et al., 2012, 2] Kuula, J., Pölönen, I., Puupponen, H-H., *Using Hyperspectral Imaging for Detecting Destructive Subjects and Materials*, NBC2012 International symposium on CBRNE Threats, Turku, Finland

[Lawson et al., 1974] Lawson, C. L., Hanson, R. J. 1974 *Solving Least Squares Problems*. Prentice-Hall

[Lee et al., 1990] Lee, J. B, Woodyatt, A. S., Berman, M. 1990. *Enhancement of High Spectral Resolution Remote-Sensing Data by a Noise-Adjusted Principal Components Transform*. IEEE Transactions on Geoscience and Remote Sensing, Vol. 28, Issue 3.

[Maxwell, 1857] Maxwell, J. C. 1857. *Experiments on Colour, as perceived by the Eye, with Remarks on Colour-Blindness*. Transactions of the Royal Society of Edinburgh, 21

[Nascimento et al., 2005] Nascimento, J. M. P., Dias, J. M. B. 2005. *Vertex component analysis: a fast algorithm to unmix hyperspectral data*. IEEE Transactions on Geoscience and Remote Sensing, Vol. 43 Issue 4.

[Plaza et al., 2005] Plaza, A., Chang, C., *An Improved N-FINDR Algorithm in Implementation*. Proc. SPIE 5806, Algorithms and Technologies for Multispectral, Hyperspectral, and Ultraspectral Imagery XI.

[Pölönen, 2013] Pölönen, I., *Discovering Knowledge in Various Applications with a Novel Hyperspectral Imager*, Jyväskylä Studies in Computing 184, University of Jyväskylä.

[Saari et al., 2009] Saari, H., Aallos, V., Akujärvi, A., Antila, T., Holmlund, C., Kantojärvi, U., Mäkynen, J., Ollila, J., *Novel Miniaturized Hyperspectral Sensor for UAV and Space Applications*, Proc. SPIE 7474, Sensors, Systems, and Next-Generation Satellites XIII.

[Williams et al., 2006] Williams, D. L., Goward, S., Arvidson, T., *Landsat: Yesterday, Today and Tomorrow*. Photogrammetric Engineering & Remote Sensing Vol. 72, No. 10

[Winter, 1999] Winter, M. E. 1999. *N-FINDR: an algorithm for fast autonomous spectral end-member determination in hyperspectral data*. Proc. SPIE 3753, Imaging Spectrometry V.

[Wollaston, 1802] Wollaston, W. 1802. *A Method of Examining Refractive and Dispersive Powers, by Prismatic Reflection*. Phil. Trans. R. Soc. Lond. vol. 92

ORIGINAL PAPERS

PI

USING VIS/NIR AND IR SPECTRAL CAMERAS FOR DETECTING AND SEPARATING CRIME SCENE DETAILS

by

Jaana Kuula, Ilkka Pölönen, **Hannu-Heikki Puupponen**, Tuomas Selander, Tapani Reinikainen, Tapani Kalenius and Heikki Saari 2012

Proceedings of SPIE Vol. 8359, Sensors, and Command, Control, Communications and Intelligence (C3I) Technologies for Homeland Security and Homeland Defense XI, 83590P (May 1, 2012); doi:10.1117/12.918555;

Using VIS/NIR and IR spectral cameras for detecting and separating crime scene details

Jaana kuula*[a], Ilkka Pölönen[a], Hannu-Heikki Puupponen[a], Tuomas Selander[a], Tapani Reinikainen[b], Tapani Kalenius[c], Heikki Saari[d]

[a]Univ. of Jyväskylä, Dept. of Mathematical Information Technology, P.O. Box 35, FI-40014 Jyväskylä, Finland; [b]National Bureau of Investigation, P.O. Box 285, FI-01301 Vantaa, Finland; [c]Central Finland Police Department, P.O. Box 59, FI-40101 Jyväskylä, Finland; [d]VTT Technical Research Centre of Finland, P.O. Box 1000, FI-02044 VTT, Finland

ABSTRACT

Detecting invisible details and separating mixed evidence is critical for forensic inspection. If this can be done reliably and fast at the crime scene, irrelevant objects do not require further examination at the laboratory. This will speed up the inspection process and release resources for other critical tasks. This article reports on tests which have been carried out at the University of Jyväskylä in Finland together with the Central Finland Police Department and the National Bureau of Investigation for detecting and separating forensic details with hyperspectral technology. In the tests evidence was sought after at an assumed violent burglary scene with the use of VTT's 500-900 nm wavelength VNIR camera, Specim's 400-1000 nm VNIR camera, and Specim's 1000-2500 nm SWIR camera. The tested details were dried blood on a ceramic plate, a stain of four types of mixed and absorbed blood, and blood which had been washed off a table. Other examined details included untreated latent fingerprints, gunshot residue, primer residue, and layered paint on small pieces of wood. All cameras could detect visible details and separate mixed paint. The SWIR camera could also separate four types of human and animal blood which were mixed in the same stain and absorbed into a fabric. None of the cameras could however detect primer residue, untreated latent fingerprints, or blood that had been washed off. The results are encouraging and indicate the need for further studies. The results also emphasize the importance of creating optimal imaging conditions into the crime scene for each kind of subjects and backgrounds.

Keywords: Spectral imaging, forensic investigation, crime scene, detection, separation of blood, latent fingerprints

1. INTRODUCTION

The first impression and detecting invisible evidence are one of the most important leads for forensic inspection when arriving at the crime scene for the first time. Critical details should also be identified as soon as possible in order to minimize the time spent on analyzing irrelevant objects. Different subjects and materials should also be separated from each other at a very early stage of the inspection, for example if the examined blood comes from two or more people. While taking and analyzing samples of the inspected targets, the original object should be kept as untouched as possible for preserving the original situation as evidence for the court and further inspection. In many cases, the analysis should also be made immediately before the samples change and degrade in the course of time.

1.1 The competitive advantage of spectral imaging

In the current inspection methods latent targets are usually made visible with the assistance of different treatments and lights, which illuminate a very small area at a time. With these kinds of methods, inspecting a whole room and all items in it is time-consuming, whereas most of the inspected surfaces will not hold anything relevant to the investigation. If something interesting is found, a sample or the whole item will be taken into a laboratory for a closer inspection. The laboratory inspection will then include various kinds of analysis, of which chemical analysis might change the sample permanently.

*jaana.kuula@jyu.fi; phone: +358-40-8053272; fax +358-14-2602209; jyu.fi

In contrast to other current inspection methods, spectral imaging does many of the same things in a shorter time and without touching or changing the inspected target. Depending on the configuration, spectral imaging may be utilized both in a laboratory and at the crime scene, of which both alternatives offer potential advantages for the forensic inspection. When spectral imaging is being used for screening the crime scene, also a great share of the analysis may be done there. Only the most critical items need to be taken into a laboratory for a deeper analysis, which will save time and speed up the performance of the whole process. In all forensic cases, the use of spectral imaging and all of its configurations are however not necessary or useful. Therefore one needs to be aware of which kinds of cases they are suitable for.

Many of the previous research support using spectral imaging in forensic inspection. To select some that are related to this research, for example Malkoff, D. and Oliver [1] refer to portable sensors in crime scene investigations. Since that especially Saari et al. [8], [9], [10] have contributed to the development of small and portable spectral imaging devices. Referring to the spectral analysis of certain kinds of samples which are tested in this study, for example Flynn et al. [2] have studied the analysis of multi-layer paint chips with hyperspectral technology. Several researchers have also contributed to the analysis of blood in its various forms. For example, Dowler [3] has studied the detection of blood, and Payne, G. and Langlois, N. [4] have specialized in studying bruises and ageing of blood. This analysis deals also with the separation of blood and other elements (bile). The detection of latent fingerprints by spectral imaging has been covered thoroughly by Tahtou et al. [5]. The article deals also with the question of detecting latent marks on challenging surfaces.

1.2 Forensic research performed by the University of Jyväskylä

The University of Jyväskylä is currently conducting a project together with the Central Finland Police Department and the Finnish National Bureau of Investigation for testing alternative spectral technologies for the detection and separation of forensic details at an assumed crime scene. The first tests were run with three different types of spectral cameras from two manufacturers. These were VTT's 500-900 nm wavelength VNIR camera [9], [10], Specim's 400-1000 nm VNIR camera [11], and Specim's 1000-2500 nm SWIR camera [12]. Spectral images were then analyzed with several kinds of mathematical algorithms for revealing the actual results of the imaging. The tests covered five different subjects which often appear but may not always be easily found at a typical murder scene or in a place of a violent burglary. These subjects were various forms of blood, gunshot residue, primer residue, fingerprints, and traces of paint, for example left by some tool that has been used in the crime.

The tests were performed indoors in plain conditions and no special forensic methods were used during the study. Additionally, the samples were not treated with any kinds of special lights or chemicals before carrying out the tests.

During the examination, slightly visible subjects like traces of paint and gunshot residue were quite easily detected with a visual inspection and near infrared cameras. These types of cameras could also separate some relevant details of the same subjects like the areas of different kinds of paint in the same objects. The same cameras could also separate burnt gunshot residue from the unburned gunpowder. The VNIR cameras could, however, not reveal subjects which are not visible for the human eye.

The infrared camera performed better with blood, which was tested in three different forms. There were dry blood stains on a ceramic plate, a mixture of four different kinds of blood absorbed in a darkish piece of cloth, and invisible trace of blood that had been wiped off a table with water and some purifying agents. The infrared camera could detect the blood which was absorbed in a piece of darkish cloth. The same camera was also able to separate the four different samples of blood, which were mixed into a same stain and absorbed in a piece of darkish cloth. Two of the samples were from two different males and one female, and one from cattle. However, the invisible subjects like fingerprints, primer residue, and the samples of blood that had been washed off, were not detectable with the infrared camera. This part of the test should, however, be repeated and improved because there were some distracting reflections of light which may have deteriorated the results in this part of the study. For example, according to Tahtou et al. [5], untreated latent fingerprints may be detected by infrared imaging only on backgrounds that are absent from interferences in the C-H bonds.

The results indicate that spectral imaging is a potential technology for revealing latent subjects at the crime scene and for separating relevant details from other subjects and materials. One should, however, be quite precise with choosing the right wavelength for each material being examined because all wavelengths do not reveal all subjects. Also the quantity of inspected materials and the concentration of liquid matters will affect the imaging results. False results may also occur when the used illumination method is not in balance with the inspection scene, camera, and target, and if there are some other external factors which affect the quality of imaging. Detecting latent marks may also be very critical with the surface on which the marks are printed and they may not be found without using some additional methods and treatments

like fluorescent lights or chemical fuming. While evaluating the economy of using spectral imaging at the crime scene, additional treatments will increase the inspection time compared with the detection and analysis of untreated marks. If, however, treatments are necessary for the detection and separation of latent marks, the grounds for using spectral imaging come from the other values of spectral analysis per se.

2. THE RESEARCH SETTING

Spectral technology is currently being used for forensic investigation purposes in laboratory environments, for which for example ChemImage Corporation has commercial applications [6]. However, the usage is not extremely widespread yet and additional research might be useful for proving its overall efficiency and impact on the police work. In this study it is assumed that spectral technology will save costs in forensic inspection and that those savings come both from the inspectors' work and from the laboratory work. Savings in the forensic inspectors' work do not however come primarily from using spectral technology in the laboratory, but from using it at the actual crime scene. Final advantages would come from reducing the lead time of inspection and analysis at the crime scene and in the laboratory, and from increasing the percentage of solved cases of all crimes and the number of solved cases within a certain period of time.

2.1 Requirements for spectral technology in the crime scene investigation

So far, there is not much reported material available of using spectral technology in the policemen's field work. For implementing spectral technology widely in this kind of work, the laboratory technology should first be developed to be compact enough so that it could be taken easily into any kind of crime scene. Regardless of the small size, the technology should reach most of the laboratory equipment's qualities so that it could easily find critical details. For being competitive and useful, it should also be able to find most of the same details which can be found with other inspection methods. It only should do it faster and better. At its best, spectral technology should be able to detect details which cannot be found with traditional methods. Also, it would be able to analyze findings without touching and changing the sample, which is a different feature compared with some other inspection methods.

2.2 Arrangements for performing the tests at an assumed crime scene

In this research, spectral technology is being tested in an assumed field environment at a proposed crime scene. For carrying out the tests, a special research setting was created for searching for latent traces of an assumed crime and for separating relevant details with different portable spectral cameras. Cameras were also equipped with some special accessories in order to enable their convenient use at the crime scene. Accessories were various stands, holders, and illuminators, but not special forensic investigation tools like fluorescent lights.

Referring to the known potential of spectral technology in forensic [1], [5], [6] and other fields like medicine [7], there were positive expectations of being able to detect invisible traces at the assumed crime scene with spectral cameras. It was, however, not known, which subjects particularly would be found, in which concentrates, and with which wavelengths. Different subjects and materials were also expected to be separated from each other, if they were mixed or absorbed into another material.

The technical potential of the spectral technology was planned to be assessed by systematic search. For carrying out the tests, a representative selection of different samples was chosen for the study, all of them representing an assumed crime scene. All samples were prepared and provided by the forensic inspectors of the Central Finland Police Department and by the personnel of the forensic laboratory of the National Bureau of Investigation.

Furthermore, three different types of spectral cameras were selected for the tests in order to find out which kinds of cameras would find the wanted details best. Two of the cameras were visual inspection and near infrared VNIR cameras and one short-wavelength IR camera. VNIR cameras were from two different manufacturers. The 500-900 nm camera was manufactured by VTT Technical Research Centre of Finland and the 400-1000 nm camera by Specim – Spectral Imaging Ltd, also located in Finland. The SWIR camera was manufactured by Specim Ltd.

The assumed crime scene was an ordinary office room, which presented a hypothetic violent burglary scene. Selected seven kinds of samples were brought into the scene, some of them being invisible for the human eye. There were also examples of washing off the trace. After imaging all the samples, spectral images were analyzed with mathematical algorithms, which then gave the actual results of the spectral imaging.

3. CARRYING OUT THE TESTS

The tests were carried out by bringing the selected samples to the assumed crime scene and by imaging them systematically with three different spectral cameras. The whole test consisted of a couple of separate imaging sessions.

3.1 Preparing the tested cameras and samples

Different cameras were used in the same imaging sessions. The cameras needed different accessories and other arrangements depending on the sample. The tested samples were not treated in any way before or during the study. A picture of VTT's VNIR camera without accessories is shown in Figure 1.

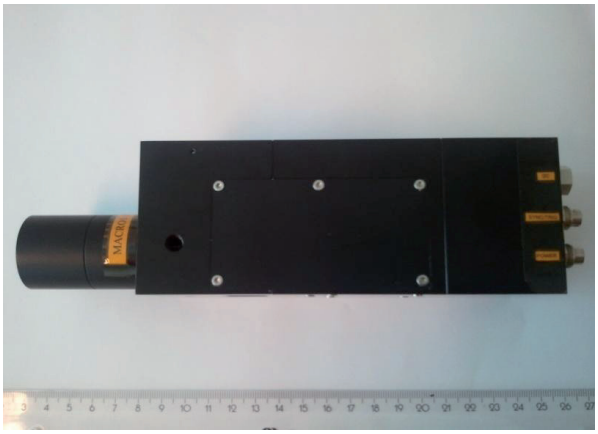

Figure 1. A picture of VTT's 500-900 nm wavelength VNIR spectral camera, which was one of the three cameras used in the tests.

The selected samples presented typical details that could be found at a violent burglary scene. These were:

- a drop of blood, dried on a ceramic plate
- invisible blood, washed with detergents and wiped off a table
- samples of four kinds of human and animal blood, mixed together and absorbed into a darkish denim fabric
- mixture of burnt and unburned gunpowder on a white paper
- invisible primer residue on an adhesive disk
- latent fingerprints on a clear plastic bag
- samples of three kinds of paint and filler, mixed on small pieces of wood.

The samples contained both easy and challenging targets in order to test the capability of different cameras and algorithms. The most challenging targets were those which were not visible for the human eye (latent fingerprints, primer residue) and which had been wiped off by using some detergent for destroying the trace (blood). Also the sample of four different bloods was quite challenging to be separated, and usually tests are performed with one or two types of blood at one time. In this part of the tests the challenge for hyperspectral imaging was to separate the mixed blood samples of two males, one female, and cattle from a single stain which was absorbed into a piece of darkish cloth. The blood stains of humans had been created from a fresh drop of blood. The animal blood had been frozen, and it was thawed before preparing the samples. The concentration of frozen blood may have been slightly weaker than what it is in fresh blood. It had, however, been frozen fresh without any additives (for example coagulation inhibitors) which makes it quite comparable with the fresh animal blood.

The sample of gunshot residue was quite rough and likely to be found and separated by spectral imaging. The primer residue was finer and more difficult to find. It was attached to an adhesive disk and the residue was not visible for the human eye. Also, the fingerprints on a clear plastic were not visible for the human eye. The last sample was a mixture of three different kinds of paint and filler which were layered on small pieces of wood. All of the subjects could not be seen with a human eye.

3.2 The course of the test

There were two kinds of performance tests for the cameras. The first question was whether they can detect such small particles that could not be observed with a human eye or which are hidden or destroyed on purpose. The second question was whether the cameras can separate subjects and materials if they are mixed, for example if various liquids are blended together, or if the liquids are absorbed into some texture, such as fabric.

Samples were at first photographed with an ordinary digital camera as reference pictures, and then imaged with the two different VNIR cameras and with the SWIR camera. If positive results were gained with VNIR cameras, SWIR imaging was not necessarily done. After imaging the samples, final results were created by analyzing spectral images with different types of mathematical algorithms. For enabling the afterward tracing of imaging sessions, all samples and images were named, classified, and registered on the project documentation. Shootings consisted of several sessions.

In some cases there were some distractions during the shootings, which may have affected the results negatively. Distractions were mainly caused by unintended reflections of light. The best positive results (separation of blood) were cross-checked and repeated twice.

4. RESULTS

The results in the tests were positive and promising but not fully successful. With some samples there were also some external factors which may have affected the results negatively. In its entirety, the whole series of tests was successful and gives support for further research.

4.1 Overview of the results

The key results of all the tested samples are presented in Table 1. The detection of the searched details and items is indicated by 'Found' or 'Not Found'. If the sample has not been imaged by a certain camera type, it is indicated by 'Not imaged'. Samples have not always been imaged with the SWIR camera if a positive result has been reached with the VNIR. The separation of mixed and absorbed items is indicated by 'Separated' or 'Not separated'. Distractions during the imaging are also indicated in the table.

Table 1. Outline of samples and results.

	RESULTS WITH VNIR CAMERAS		**RESULTS WITH SWIR CAMERA**
SAMPLE	**VTT VNIR 500-900 nm**	**Specim VNIR 400-1000 nm**	**Specim SWIR 1000-2500 nm**
BLOOD			
- Dried blood on a ceramic plate	Found	Found	Not imaged
- Invisible blood, wiped off a table	Not found, noise	Failed, reflections	Not possible with equipment available
- Mixture of four types of blood, absorbed in a darkish cloth	Found, not separated	Found, not separated	Found and separated 4 different types of blood
GUNSHOT RESIDUE			
- A mixture of burnt and unburned gunpowder on a white paper	Found and separated	Not imaged	Not imaged
PRIMER RESIDUE			
- Invisible residue on an adhesive disk	Not found	Not found	Not imaged
FINGERPRINTS			
- Invisible fingerprints on a clear plastic bag	Not found	Not found	Failed, reflections
PAINT			
- Three different paints and fillers mixed on a piece of wood	Found and separated 3 of 4 mixed samples	Found and separated 3 of 4 mixed samples	Found and separated 4 mixed samples

4.2 Results in detecting items

When detecting interesting items, the best results were obtained in finding blood and paint. Of these single blood stains were found with all of the three tested camera types. All cameras could also find the paint and gunpowder. (Gunpowder was imaged only with 500-900 nm VNIR, but it was evident that it would be found also with the other cameras.) These samples were quite easy to find, so with these kinds of items it is more critical whether the cameras are able to separate different items from the mixed and absorbed samples.

None of the cameras could however detect items which were invisible for the human eye. The invisible items were the blood which had been wiped off a table by using some detergents during the cleaning, primer residue which was attached to an adhesive disk, and latent fingerprints on a clear plastic bag. The trace of blood had been destroyed on purpose and in the imaging of primer residue and fingerprints on a clear base there were some reflections of light which may have distracted the imaging process. Due to these reasons the detection of these invisible and latent samples was very challenging, and it is not surprising that no traces could be found.

It is however possible that in more favorable conditions the SWIR camera might be able to detect invisible blood and other traces invisible for the human eye. The detection of the destroyed trace is dependent among other things on the cleaning method, usage of detergent, and the strength of the trace which has been left on the scene after the cleaning. The detection of latent items might also be possible on some other than a clear plastic base, and with some other wavelengths and better spectral resolution. Referring to Tahtou et al. [5], especially untreated latent fingerprints might be detected by imaging the spectral intensity at a single frequency (non-chemical imaging) or imaging them with infrared frequencies on backgrounds that are absent from interferences in the C-H region (chemical imaging). Tahtou et al. have also imaged latent fingerprints by treating them first with Ethyl Cyanoacrylate fuming [5]. This will make latent prints imageable, but increasing these kinds of additional processes in the work load of the investigators might increase the total time spent on investigation at the crime scene and make the whole examination process more complicated. One must then evaluate the value of the quality of inspections compared with the time spent on each investigation, and decide between the appropriate research methods accordingly. To summarize, latent marks and residue are subjects where further research is in any case necessary.

4.3 Results in separating items

In separating mixed and absorbed items, the cameras were expected to detect four different kinds of blood which were mixed into the same stain and absorbed into a darkish cloth. Also the burnt and unburnt gunpowder were supposed to be separated, as well as the three kinds of paint and filler which were on the same pieces of wood. The different types of blood and the three types of paint and filler could not be separated with a human eye.

The VNIR cameras could separate the burnt and unburnt gunpowder, as well as three of the four items of paint and filler on the small pieces of wood. The gunpowder was quite easy to observe and the burnt and unburnt grains were clearly seen in spectral images. The VNIR image of separating burnt and unburnt gunpowder is shown in Figure 2.

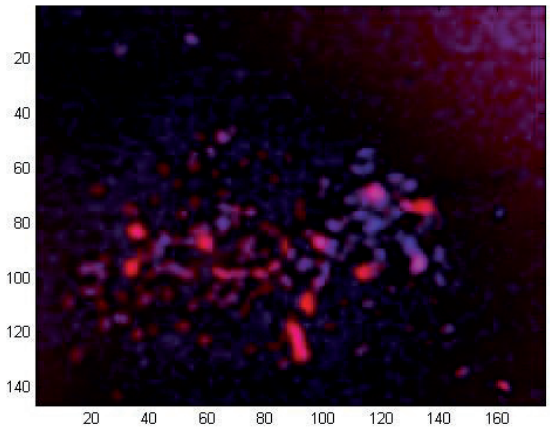

Figure 2. Visualization of separating burnt and unburnt gunpowder based on a processed VNIR datacube.

While examining the painted pieces of wood with VNIR cameras, spectral imaging could separate three of the four items on the wood. The two identified items were green and white paint, whereas the third item which was identified as one, consisted of filler and a black marker pen. The VNIR image of separating three types of paint and filler is presented in Figure 3.

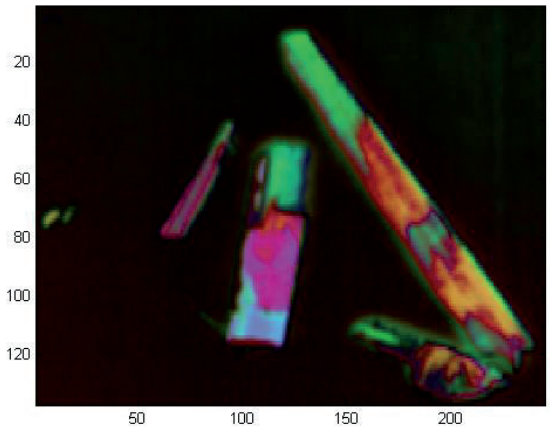

Figure 3. Visualization of the separation of mixed paint and filler on pieces of wood based on a processed VNIR datacube.

The SWIR camera succeeded best in separating mixed and absorbed items, and as the best result of the whole test it could separate the four types of blood which were mixed in the same stain and absorbed in a piece of darkish cloth. The SWIR camera could also separate all four materials on the pieces of wood. Compared to VNIR cameras, SWIR camera performed better in separating the filler and the black marker pen. While the VNIR camera recognized these two items as one, the SWIR camera detected the trace of the black marker pen different from the filler. A processed SWIR PCA RGB

composite image of the mixed paint and filler with three principal components is shown in Figure 4 and a SWIR pseudo color image of the same target in Figure 5.

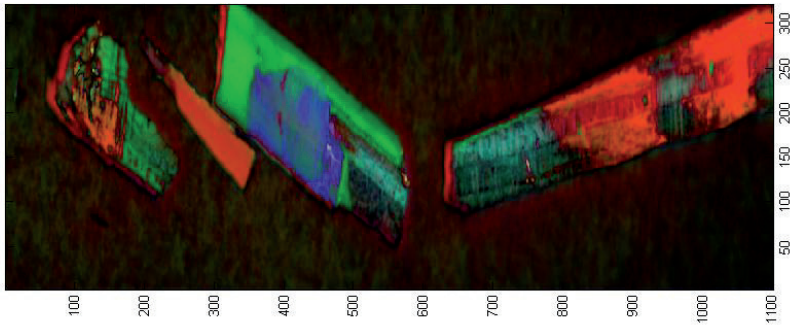

Figure 4. A processed SWIR PCA RGB composite image with three principal components of the separation of mixed paint and filler on pieces of wood.

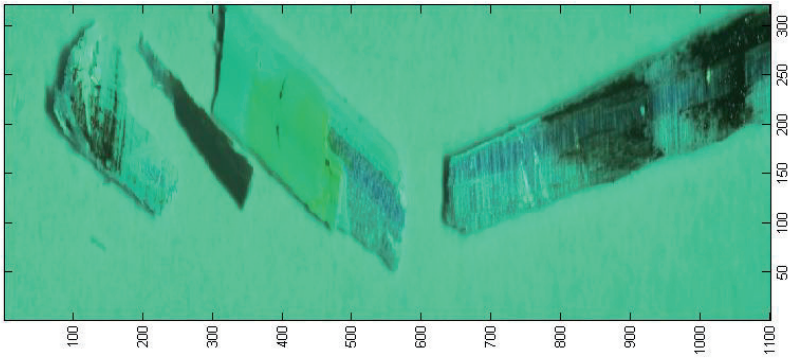

Figure 5. A SWIR pseudo color image of the separation of mixed paint and filler on pieces of wood.

Figures 6-8 present the separation process of four types of blood with digital, VNIR, and SWIR cameras. Figure 6 shows the reference picture of the stain which contains blood from two different males, one female, and one cattle animal. From the picture one cannot tell how many persons' or animals' blood there is in the same stain. In Figure 7 there is a visualization based on a processed VNIR datacube of the same sample, and that cannot indicate how many persons' or animals' blood there is in the stain, either.

The full separation of the four blood types is shown in Figure 8. The successful result is based on imaging the stain with the SWIR camera and on processing images with the right kind of algorithms. Figure 8 presents the visualization of the examined stain based on a processed SWIR datacube.

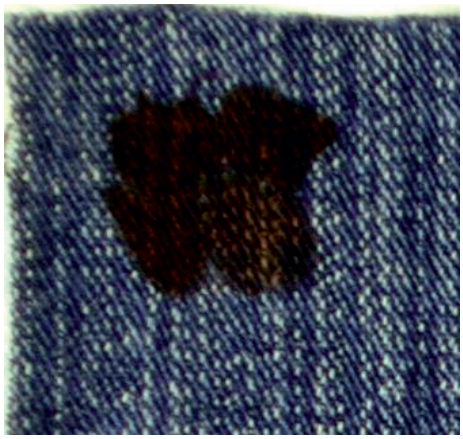

Figure 6. Reference picture of four different types of blood mixed in the same stain and absorbed in a denim cloth.

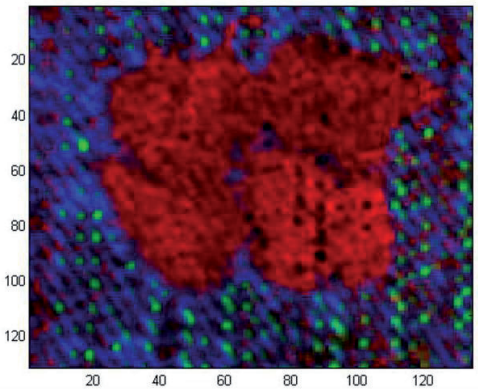

Figure 7. VNIR image of four different types of blood mixed in the same stain and absorbed in a denim cloth.

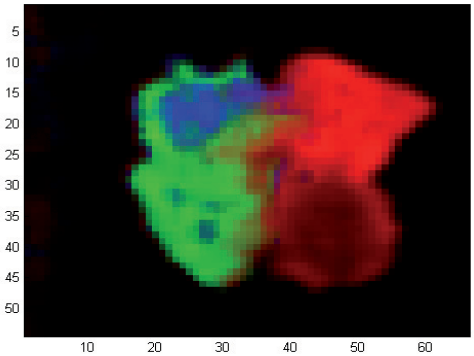

Figure 8. Visualization of four different types of blood mixed in the same stain and absorbed in a denim cloth based on a processed SWIR datacube.

5. SUMMARY AND CONCLUSIONS

In the University of Jyväskylä's research project the aim is to bring spectral imaging technologies from the laboratory into the crime scene as the policemen's help in forensic inspection work. The motivation for using spectral imaging at the crime scene is to detect and separate relevant items better and faster compared with other inspection methods. Improved and faster inspection should also cut down the time spent in examining each case of crime. As the result of more qualified detection and separation of relevant details, faster inspection times as well as the overall percentage of solved cases and the number of solved cases within a certain period of time should increase.

Within this study, three kinds of spectral cameras were tested for detecting and separating interesting items at an assumed crime scene of a violent burglary. The tests were run with VTT's 500-900 nm VNIR camera, Specim's 400-1000 nm VNIR camera, and Specim's 1000-2500 nm SWIR camera. All of these cameras were used for detecting and separating samples which were related to the assumed violent burglary. The tested samples were the following: dried blood on a ceramic plate, invisible blood which had been wiped off a table with detergents, a sample of four types of human and animal blood which were mixed into the same stain and absorbed into a darkish fabric, a mixture of burnt and unburnt gunpowder, primer residue, latent fingerprints on a clear plastic bag, and a sample of three kinds of paint and filler on small pieces of wood.

The tests showed that the VNIR cameras can detect visible samples and separate some items which are mixed together. For example, VNIR cameras can separate various types of paint on the same object. However, in these tests VNIR cameras could not detect or separate items that are invisible for the human eye. Additional research is therefore recommended on the detection of very small particles and latent objects.

The tests also showed that the SWIR camera is better than the VNIR cameras in detecting and separating various items. For example, unlike VNIR cameras the SWIR camera was able to detect and separate four different types of blood which were mixed into the same stain and absorbed into the darkish piece of cloth. The SWIR camera could also detect and separate the three types of paint and filler on the piece of wood. Based on these results it is suggested that additional research would be done on the detection and separation of blood with the spectral technology.

The results of the study are encouraging and it is suggested that additional research will be made on developing the use of spectral imaging in the forensic field. Especially the equipment and research methods related to the use of spectral technology at the crime scene are worth studying further. The spectral imaging technology especially in the VNIR spectral range will lead to devices which are similar in size to compact digital cameras [13]. Improvements may also be achieved with the laboratory equipment. As a conclusion, development on both the laboratory equipment and the field inspection methods will reduce the workload of forensic inspectors, policemen, and criminal laboratory workers as well as enable solving more criminal cases in a shorter period of time.

6. ACKNOWLEDGEMENTS

We would like to acknowledge Tekes – the Finnish Funding Agency for Technology and Innovation and the University of Jyväskylä for funding this research project called *Crime Scene Investigations by Spectral Imaging –SpeCSI* (2623/31/2011). TEKES has funded 60 % and the University of Jyväskylä 40 % of the project.

REFERENCES

[1] Malkoff, D. and Oliver, W.R., "Hyperspectral imaging applied to forensic medicine", Proc. SPIE 3920, 108 (2000)

[2] Flynn, K., O'Leary, R., Lennard, C., Roux, C. and Reedy, B. J., "Forensic Applications of Infrared Chemical Imaging: Multi-Layered Paint Chips", J Forensic Sci, July 2005, Vol. 50, No. 4

[3] Dowler, S. W., [Applications of Hyperspectral Imaging Techniques to Forensic Image Analysis], A thesis submitted in partial fulfilment of the requirements for the degree of Doctor of Philosophy in Electrical Engineering, The University of Auckland (2010)

[4] Payne, G. and Langlois, N., "Applying visible hyperspectral (chemical) imaging to estimate the age of bruises", *Med Sci Law July 2007 vol. 47 no. 3 225-232*
[5] Tahtouh,M., Kalman, J. R., Roux,C., Lennard,C. and Reedy,B.J., "The Detection and Enhancement of Latent Fingermarks Using Infrared Chemical Imaging", J Forensic Sci, Jan. 2005, Vol. 50, No. 1
[6] "Forensic analysis", www.chemimage.com/markets/forensics/
[7] Seong G. Kong, S. and Park, L., [Hyperspectral Image Analysis for Skin Tumor Detection], Springer (2009)
[8] Saari, H., Aallos, V., Akujärvi, A., Antila, T., Holmlund, C., Kantojärvi, U., Mäkynen, J. and Ollila, J., "Novel Miniaturized Hyperspectral Sensor for UAV and Space Applications", Proc. SPIE 7474 (2009).
[9] Saari, H., Aallos, V., Holmlund, C., Malinen, J., Mäkynen, J., "Hand-Held hyperspectral imager," Proc. SPIE 7680, 76800D (2010)
[10] Saari H., "Spectrometer and interferometric method", US Patent US 8,130,380 (Mar. 6, 2012)
[11] Data sheet of Specim VNIR Spectral Camera www.specim.fi/media/specam-datasheets/ps-spectral-camera-v1-11.pdf
[12] Data sheet of Specim SWIR Spectral Camera www.specim.fi/media/specam-datasheets/swir-specam-ver3-11.pdf
[13] Antila, J., Mannila, R., Kantojärvi, U., Holmlund, C., Rissanen, A., Näkki, I., Ollila, J:, and Saari, H., "Spectral imaging device based on a tuneable MEMS Fabry-Perot interferometer", to be published in Proc. SPIE 8374, 8374-15 (2012).

PII

THE CHALLENGES OF ANALYSING BLOOD STAINS WITH HYPERSPECTRAL IMAGING

by

Jaana Kuula, **Hannu-Heikki Puupponen**, Heikki Rinta, Ilkka Pölönen 2014

Proc. SPIE 9112, Sensing Technologies for Global Health, Military Medicine, and Environmental Monitoring IV, 91120W (5 June 2014); doi: 10.1117/12.2050180

The challenges of analysing blood stains with hyperspectral imaging

Kuula J.[a], Puupponen H-H.[a], Rinta H.[b], Pölönen I.[a],

[a]Department of Mathematical Information Technology, University of Jyväskylä, Mattilanniemi 2, 40100 Jyväskylä, Jyväskylä, Finland;
[b]Department of Chemistry, University of Jyväskylä

ABSTRACT

Hyperspectral imaging is a potential noninvasive technology for detecting, separating and identifying various substances. In the forensic and military medicine and other CBRNE related use it could be a potential method for analyzing blood and for scanning other human based fluids. For example, it would be valuable to easily detect whether some traces of blood are from one or more persons or if there are some irrelevant substances or anomalies in the blood. This article represents an experiment of separating four persons' blood stains on a white cotton fabric with a SWIR hyperspectral camera and FT-NIR spectrometer. Each tested sample includes standardized 75 μl of 100 % blood. The results suggest that on the basis of the amount of erythrocytes in the blood, different people's blood might be separable by hyperspectral analysis. And, referring to the indication given by erythrocytes, there might be a possibility to find some other traces in the blood as well. However, these assumptions need to be verified with wider tests, as the number of samples in the study was small. According to the study there also seems to be several biological, chemical and physical factors which affect alone and together on the hyperspectral analyzing results of blood on fabric textures, and these factors need to be considered before making any further conclusions on the analysis of blood on various materials.

Keywords: hyperspectral analysis, analysis of blood

1. INTRODUCTION

The forensic and military medicine, forensic investigations and various screenings in the CBRNE field require quick and nonivasive methods for having an overview of the state and constitution of blood and other biological fluids. The hyperspectral analysis is known of its ability make untouched basic analyses of the structure and content of the selected targets. It is, however, unclear whether it would be able to detect, identify and separate small particles in blood and in other body fluids. The small particles may refer to the healthy or abnormal components and structure or to the foreign substances in blood.

In this research the hyperspectral analysis has been focusing on the constitution and structure of blood in order to find out whether two or more people's blood can be separated by hyperspectral technology and in which factors this separation would be based on. If the basic elements and structure of blood could be detected by common hyperspectral technologies, one might assume that also some inappropriate substances and anomalies in blood could be detected with the same technology.

In the earlier study[1] four different blood samples, one from female, two from different men and one from cow, were separated successfully with a 1000-2500 nm SWIR type of hyperspectral camera. It was, however, not revealed, which factor or factors in blood caused the differences for being able to define the samples as different blood.

In this article the earlier study has been repeated with new carefully produced and analyzed blood samples from four people for explaning why different persons' blood shows up different in hyperspectral analysis. In this test the hyperspectral analysis has been supported with an additional analysis of the structure of blood made by professional medical personnel and equipment.

Further author information:
Jaana Kuula: E-mail: jaana.kuula@jyu.fi, Telephone: +358 40 8053272

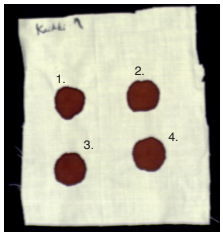

Figure 1. Four persons blood stains on cotton fabric.

The new tests support the earlier findings of being able to separate different persons' blood with hyperspectral analysis. The results also indicate slightly that the erythrocytes might be the explaining factor for the separation of blood. It should, however, be noted that the sample size in this study is small (n=4) and thus no statistically meaningful conclusions can be drawn. Instead, further in the paper we concentrate on describing the utilized analyzing method and on the potential for further study in this subject.

2. METHOD

2.1 Research design and preparation of samples

The tests were started by taking pure blood samples from four healthy volunteers by professional healthcare personnel. The volunteers were about 25-50 years of age, three men and a woman. All were non-smokers and had never used drugs. They also had not eaten, drunk or taken any alcohol in 12 hours before giving blood. In the laboratory a blood count was made on the samples. 8 ml of blood was taken from each volunteer and the blood samples were stored refrigerated for two days before sample preparation. The results from laboratory tests are presented in Table 1 and an image of the tested blood stains on cotton fabric in Figure 1.

Table 1. Measured blood constituents and correlations between identified spectra's mutual spectra angle matrix and distance matrix of measured component.

Blood component	Person 1	Person 2	Person 3	Person 4	Correlation
Leukocytes $*10^9$/l	3.2	6.9	4.9	6	0.32
Erythrocytes $*10^{12}$/l	4.87	4.29	5	5.17	**0.74**
Hemoglobin g/l	153	133	147	146	0.5
Thrombocytes $*10^9$/l	161	268	239	278	0.24
Basophils $*10^9$/l	0	0	0	0.1	0.23
Eosinophils $*10^9$/l	0	0.1	0.1	0.1	0.26
Neutrophils $*10^9$/l	1.8	4.5	2.7	3.9	0.35
Lymphocytes $*10^9$/l	1.2	1.9	1.5	1.4	0.47
Monocytes $*10^9$/l	0.3	0.4	0.5	0.5	0.49

Blood stains were deposited on pieces of cotton fabric. The cotton fabric was selected to present commonplace non-bleached fabric. The base fabric was washed and ironed before the sample preparation took place. Volume of 75 μl was placed on the fabric with automatic pipette and allowed to dry off on rack in normal room temperature. Function of the rack was preventing direct contact between any surface and wet opposite side of the fabric before samples were fully dry. Off-white cotton fabric was chosen to provide a moderate background contrast. Blood stain samples had a diameter of approximately 7 mm on cotton fabric base.

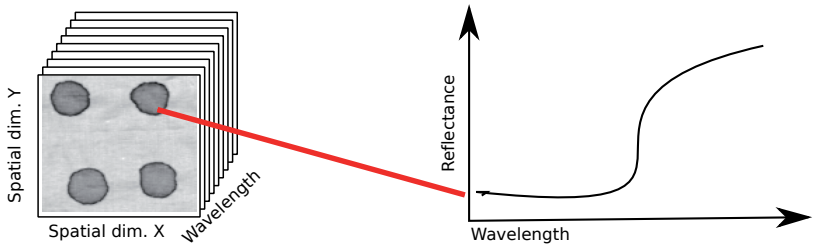

Figure 2. Illustration of hyperspectral image. Spectral image is stack of grayscale intensity images. Each spatial pixel in stack forms reflectance spectrum.

2.2 Hyperspectral imaging and analysis method

As the term indicates, hyperspectral imaging combines spectroscopy with imaging techniques. In hyperspectral data cube each pixel forms spectrum trough data cube as illustetrated in Figure 2. For the imaging we used Specim Ltd's short-wave infrared imager (SWIR), which is capable of capturing spectral data from 1000 to 2500 nm.

In paper[1] we examined various stains and materials, which could be identified at a crime scene. In the study we were also able to separate blood stains originating from three different persons and one animal from each other. The analysis was performed with vertex component analysis[2] and inversion was computed with non-negative least squares algorithm.[3] These algorithms are utilized also in this study.

Basic idea behind vertex component analysis is that imaged spectra are linear mixture of pure spectra, often termed endmembers. Vertex component analysis determines these endmembers from the vertices of the convex hull of measured data points. Method is sensitive to the number of endmembers to be extracted. This number has to be estimated before running VCA.

Spectral angle mapper (SAM)[4]is a method to compare different spectra with each other. It measures spectral similarity by finding the angle (in radians) between reference spectrum $\mathbf{e} = (e_1, e_2, \dots e_L)^T$ and imaged spectrum $\mathbf{s} = (s_1, s_2, \dots s_L)^T$ so that,

$$d_{sam}(\mathbf{e}, \mathbf{s}) = \cos^{-1}\left(\frac{\sum_{l=1}^{L} e_l s_l}{(\sum_{l=1}^{L}(e_l)^2)^{1/2}(\sum_{l=1}^{L}(s_l)^2)^{1/2}}\right),$$

where L is number of wavebands in spectra. Because we are here dealing with four samples it is possible to calculate a distance matrix, through use of SAM to determine degree of difference between each sample spectra.

Because we also had laboratory analysis performed on the blood samples, we can calculate different distance matrices with results from different samples. After this calculation it is possible to compute correlations between these distance matrices to find interpretative factors between the samples. With the correlation information it is possible to draw conclusions about what the potential cause is for the differences in the measured spectra from each blood stain.

2.3 ATR NIR spectroscopy measurements

The near infrared spectral measurements of the blood stain samples on the fabrics were measured on a Thermo Fisher Scientific Antaris II FT-NIR spectrometer using the basic measurement mode (range 10000-4000 cm $^{-1}$/ 1000-2500 nm; resolution 4 $^{-1}$cm and scans 32). Data collection was processed by OMNIC 9 -software and the collected data was processed by TQ Analyst and Microsoft Excel 2010 software. The average spectrum of the samples was a measurement of three replicates.

Measurement results varied depending on the spatial location on the spot. With spectroscopy it was not possible to separate blood stains from each other.

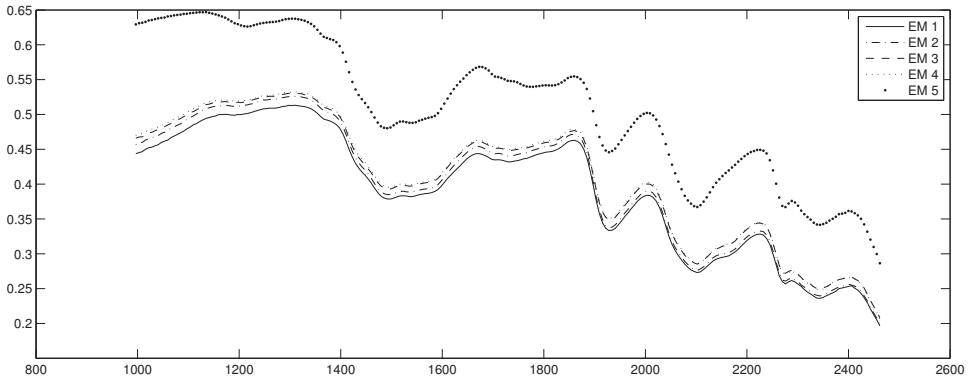

Figure 3. Endmembers inducted with VCA.

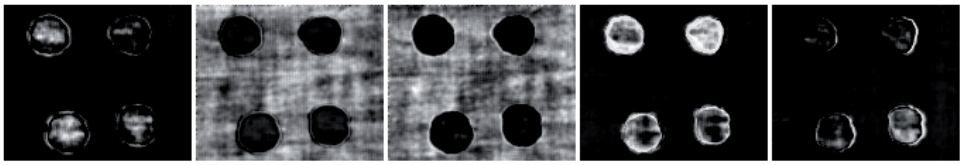

Figure 4. Abundance images of extracted endmembers. VCA fails to discover four different traces. However, it seems that stains on the right side differ from other two.

3. RESULTS

Fully dry blood stains were imaged after a couple of days from sample preparation.

As in Kuula et. al.[1] we strived to repeat the earlier excellent blood stain separation results. In this case, we were less successful. Figure 3 displays extracted endmembers and Figure 4 shows abundance maps calculated for these endmembers. It would appear that stains 2 and 4 have components, which cause them to differ from others.

Next we examined another possible approach. We selected pixels from each stain and calculated average of these pixel spectra to derive a representative single spectrum for each of the four stains. In Figure 5 we see four different spectra, which all differ from each other. It seems that there are slight differences in the relative intensity of the spectra over the whole wavelength range.

If we visually compare known strong wavebands for blood components in Table 2 with calculated mean values for each stain, presented in Figure 5, it seems clear that there are no noticeable peaks which would explain the differences.

Inversion can be calculated also for these spectra. If we add mean value of the background fabric to the group of mean spectra we obtain abundance images that all differ from each other and also give slightly different spatial distribution for each spectrum. This is illustrated in Figure 6.

We are next looking for an explanation as to why these differences appear. We have the laboratory results for the four blood samples in Table 1. One possibility is to examine if distances between these values could correlate with a distance matrix calculated from the mean stain spectra. This is relevant because each value in Table 1 and each mean spectra can be identified with a certain person.

We can build a distance matrix based on spectral angle mapper between these mean value spectra. This

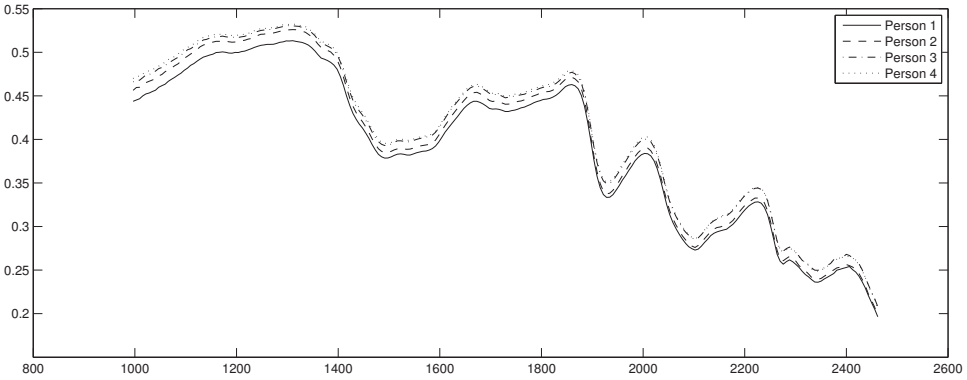

Figure 5. Mean values of the spectra, which are taken from different samples.

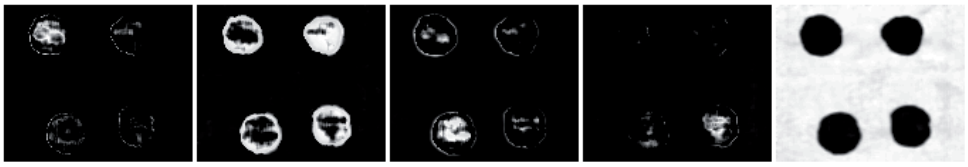

Figure 6. Non-negative least square inversion-provided abundance maps for the mean value spectra.

distance matrix of the four mean blood stain spectra is

$$D_{sam} = \begin{bmatrix} 0 & 0.0051 & 0.0065 & 0.0062 \\ 0.0051 & 0 & 0.0094 & 0.0086 \\ 0.0065 & 0.0094 & 0 & 0.0026 \\ 0.0062 & 0.0086 & 0.0026 & 0 \end{bmatrix}$$

Distance matrices D_{comp} for each component was calculated based on L2-norm. Now correlation coefficient is calculated between D_{sam} and D_{comp} following:

$$r = \frac{\sum_n \sum_m (D_{sam,n,m} - \overline{D}_{sam})(D_{comp,n,m} - \overline{D}_{comp})}{\sqrt{(\sum_n \sum_m (D_{sam,n,m} - \overline{D}_{sam})^2)(\sum_n \sum_m (D_{comp,n,m} - \overline{D}_{comp})^2)}}$$

In the last column of 1 we see these correlations. It seems that highest correlation was with erythrocyte's distance matrix

$$D_{eryth.} = \begin{bmatrix} 0 & 0.3364 & 0.0169 & 0.09 \\ 0.3364 & 0 & 0.5041 & 0.7744 \\ 0.0169 & 0.5041 & 0 & 0.0289 \\ 0.09 & 0.7744 & 0.0289 & 0 \end{bmatrix}.$$

4. DISCUSSION AND CONCLUSION

As Figure 7 illustrates there exists a possibility to distinguish the blood stains from each other. It seems that spectral similarity of mean values of these stains correlates with the amount of erythrocytes in blood. This would seem to be reasonable, as the amount of red blood cells also affects the optical properties of the blood. Greater amounts of erythrocytes would also result in darker and thicker blood. It could be possible to through

Table 2. Typical features expressed by the human blood in SWIR -region.

Wavelength (nm)	Component	Bond
930	Oxyhemoglobin	3. overtone of -CH and -CH2 stretching vibrations
970	Water	Combination of H-O-H symmetric and asymmetric
1454	Water	Combination of H-O-H symmetric and asymmetric
1690	Hemoglobin, albumin, globulin	1. overtone of -CH stretching vibrations
1740	Hemoglobin, albumin, globulin	1. overtone of band at 3477 nm
1940	Water	Combination of H-O-H bending and asymmetric stretching vibrations
2056	Hemoglobin, albumin, globulin	Combination of amide A and amide II or another
2170	Hemoglobin, albumin, globulin	Combination of amide B and amide II or
2170		overtone of amide II
2290	Hemoglobin, albumin, globulin	-CH stretching and deformation combinations
2350	Hemoglobin, albumin, globulin	-CH stretching and deformation combinations

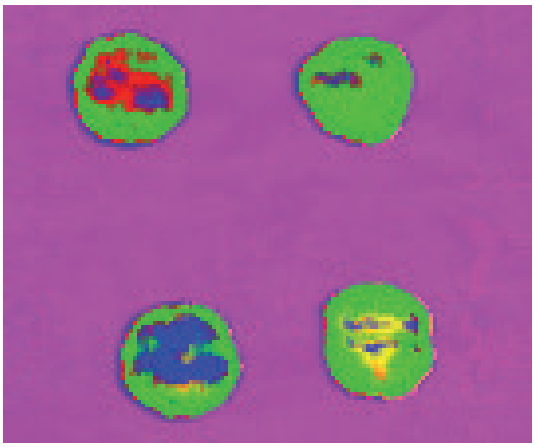

Figure 7. False color illustration of mean value spectra's abundance. There is a visual difference in each stain.

use of hyperspectral imaging to estimate erythrocyte content from blood stains and that way potentially offer an alternative for hemocytometer. At the accuracy level of erythrocytes there might also be a chance to detect other substances and phenomena in blood, althogh they were not available in the samples which were used in this study.

Although these results are interesting, they have not been confirmed statistically due to the small size of the sample. Also some possible sources of error which can affect the results were not eliminated. One of these is the background material. Although waved tightly, a cotton fabric as a basis for highly accurate optical analysis might not be sufficiently homogenous, and therefor there might be a possibility for error, caused by the physical properties of the texture. Imaging instruments might also be capturing geometry, so that if we rotated the samples 90 degrees, would the results remain the same? Based on these tests it seems possible to separate blood stains originating from one person from ones originating from another. However, based on these tests we cannot

be certain on the degree of accuracy the measuring results, so we recommend that the tests would be repeated with a much higher number of samples. Also, as there is a need to detect other anomalies in the blood, further research is needed to confirm whether they can be detected or not.

ACKNOWLEDGMENTS

This research has been funded by the Finnish Funding Agency for Innovation and by the University of Jyväskylä.

REFERENCES

[1] Kuula, J., Pölönen, I., Puupponen, H.-H., Selander, T., Reinikainen, T., Kalenius, T., and Saari, H., "Using vis/nir and ir spectral cameras for detecting and separating crime scene details," *Proc. SPIE* **8359**, 83590P–83590P–11 (2012).

[2] Nascimento, J. and Dias, J., "Vertex component analysis: A fast algorithm to unmix hyperspectral data," *IEEE Transactions on Geoscience and Remote Sensing* **34**(4), 898–910 (2005).

[3] Bro, R. and De Jong, S., "A fast non-negativity-constrained least squares algorithm," *Journal of Chemometrics* **11**(5), 393–401 (1997).

[4] Schowengerdt, R. A., [*Remote Sensing, Third Edition: Models and Methods for Image Processing*], Academic Press, Inc., Orlando, FL, USA (2006).

PIII

DETECTING EXPLOSIVE SUBSTANCES BY THE IR SPECTROGRAPHY

by

Jaana Kuula, **Hannu-Heikki Puupponen**, Heikki Rinta, Ilkka Pölönen, Marko Haukkamäki, Tuomas Teräväinen 2014

Proc. SPIE 9073, Chemical, Biological, Radiological, Nuclear, and Explosives (CBRNE) Sensing XV, 90730Q (10 June 2014); doi: 10.1117/12.2050157

Detecting explosive substances by the IR spectrography

Kuula J.[a], Rinta H.[b], Pölönen I.[a], Puupponen H-H.[a], Haukkamäki M.[c], Teräväinen T.[d],

[a]Department of Mathematical Information Technology, University of Jyväskylä, Mattilanniemi 2, 40100 Jyväskylä, Jyväskylä, Finland;
[b]Department of Chemistry, University of Jyväskylä
[c]Air Force Command Finland
[d]Central Finland Police Department

ABSTRACT

Fast and safe detection methods of explosive substances are needed both before and after actualized explosions. This article presents an experiment of the detection of three selected explosives by the ATR FTIR spectrometer and by three different IR hyperspectral imaging devices. The IR spectrometers give accurate analyzing results, whereas hyperspectral imagers can detect and analyze desired samples without touching the unidentified target at all. In the controlled explosion experiment TNT, dynamite and PENO were at first analyzed as pure substances with the ATR FTIR spectrometer and with VNIR, SWIR and MWIR cameras. After three controlled explosions also the residues of TNT, dynamite and PENO were analyzed with the same IR devices. The experiments were performed in arctic outdoor conditions and the residues were collected on ten different surfaces. In the measurements the spectra of all three explosives were received as pure substances with all four IR devices. Also the explosion residues of TNT were found on cotton with the IR spectrometer and with VNIR, SWIR and MWIR hyperspectral imagers. All measurements were made directly on the test materials which had been placed on the explosion site and were collected for the analysis after each blast. Measurements were made with the IR spectrometer also on diluted sample. Althogh further tests are suggested, the results indicate that the IR spectrography is a potential detection method for explosive subjects, both as pure substances and as post-blast residues.

Keywords: Hyperspectral detection and analysis, IR spectrography, explosives

1. INTRODUCTION

Fast and safe detection methods are needed for managing cbrne threats and their consequences during the state of war and other sudden disasters in more stable areas. This article represents an experiment were hyperspectral analysis and IR spectrography were used for identifying various explosives as pure substances and for detecting explosive residues after the blast. The motivation for the experiment was to find out whether the hyperspectral imaging technology could be used for detecting IEDs and HMEs or their carriers or builders prior to an explosion, and for detecting and identifying explosive residues after an accidental or intentional blast.

The experiment was designed and built jointly by the researchers of the Department of Mathematical Information Technology and Department of Chemistry of the University of Jyväskylä, and by the explosives specialists of the Central Finland Police Department, the bomb squad of the Finnish Police, and of the Finnish Air Force. The experiment was built to simulate a shopping mall attack, though carried out in controlled outdoor conditions. During the experiment four sequential explosions were carried out with a similar design with powder, TNT, dynamite and PENO, of which the results of TNT, dynamite and PENO are reported in this article. The residues of the explosions were caught on ten different surfaces and objects which were placed identically around the seat of the explosion in all four cases. The materials of these sample collectors were cotton fabric (in three distances), laminate, plastic carpet, detonator wire, duct tape, concrete, plastic bucket and cardboard box. Before the explosions, small samples of the pure substances were also preserved on a clean cotton cloth for the identification with the IR devices.

Further author information:
Jaana Kuula: E-mail: jaana.kuula@jyu.fi, Telephone: +358408053272

After the explosion tests all samples were analysed with the ATR FTIR spectrometer and with VNIR, SWIR and MWIR hyperspectral cameras. The ATR FTIR spectrometer was used as a comparative technology for the hyperspectral analysis and for crosschecking which samples have residues and which possibly not. Samples of pure explosives were analysed at first for recording their spectra. After that explosive residues were searched from the ten collectors which were set on the explosion scene in advance for that purpose. Samples were at first analysed with the IR spectrometer, which is a more accurate analyzing method than the hyperspectral analysis. However, for making the IR spectrometer analysis samples may need to be prepared by rinsing the explosive residues with a neutral liquid, which makes the detection of explosives and residues more complicated. After the IR spectrometer analysis collectors were imaged with VNIR, SWIR and MWIR hyperspectral cameras, after which hyperspectral data was analysed with an analyzing software.

The results show that the spectra of TNT, dynamite and PENO can be recorded from pure substances with the IR spectrometer, and that these explosives may be identified and separated with this technology. The explosive residues were, however, found only for TNT. Some of these findings were made by measuring the sample directly on the collector, and some others by measuring the rinsed sample.

The spectra of TNT, dynamite and PENO were also received with all hyperspectral camera types, which means that these three explosives can be identified and separated with VNIR, SWIR and MWIR cameras. Also the post-blast residues were found with all of these three cameras, but only for TNT and not for the two other explosives. All findings of residues which were made with hyperspectral cameras were measured directly from the collector materials which were picked up from the explosion site after each blast.

2. EXPERIMENT

2.1 Research setup

Explosion tests were performed in winter time outdoor conditions by the Department of Mathematical Information Technology and Department of Chemistry of the University of Jyväskylä with the help of the explosives specialists of The Finnish Defence Forces, Bomb Squad of the Finnish Police and the crime scene investigation group of the Central Finland Police Department. For performing the tests, 125-200 grams of TNT, dynamite and PENO were reserved as explosives and various other materials as collectors for the explosion residues. As the explosions were meant to simulate a shopping mall attack, the collector materials were chosen so that they would be likely to be found in a real target of an malicious attack. For example, concrete, laminate and plastic carpet represented the construction and cotton fabric the interior decoration of an attacked building. Accordingly, the plastic bucket, cardboard box, detonator wire and duct tape represented a homemade bomb and its container.

The design of the controlled explosion is presented in Figure 1. The explosive charge was placed in the middle and the ten sample collectors around it at various distances in the range of two meters. All collectors were of different materials, except the cotton fabric which was set on wooden racks at 1, 1.5 and 2 meters from the explosive charge. The cotton fabrics, plastic bucket and cardboard box were placed vertically and the other materials horizontally towards the center of the explosion. The post-blast situation of the explosion site is presented in Figure 2.

The explosive materials in the experiment were 200 grams of Trinitrotoluene (TNT), 125 grams of Dynamite (EGDN-based)and 200 grams of PENO (PENT-based explosive). All explosive materials were used and handled by authorized professionals.

2,4,6-trinitrotoluene (TNT) is a military explosive and it is widely used in various munitions like in mines and grenades. It is being used also as a pure explosive material. The used TNT was obtained as yellow flakes in a tight plastic bag. The used dynamite was a Forcit's FORDYN-trademark and it is an ethylene glycol dinitrate (EGDN) based ammonium nitrate (AN) explosive. FORDYN consist 30-35 % EGDN, < 2 % cellulose nitrate and 50-60 % AN. It is especially suitable for underwater mining and small-amount blasting. PENO is also a trademark of the Forcit Group and it is a plastic explosive for the military purposes. PENO is mainly used for military demolition tasks and for the disposal of unexploded ordnances (UXO). The main components of PENO are the explosive compound pentaerythritol tetranitrate (PENT) and oil. Dimetyldinitrobutan (DMDNB) was added 1 % to PENO for the post-blast identification of the used explosive.[1–4]

Sample material / target	Distance
Cotton fabrics (50*50cm)	1; 1,5 and 2 m
Plastic bucket	< 1.5 m
Cardboard box	< 1.25m
Detonator wire	-
Wiping sample (concrete)	< 0.8 m
Duct tape	< 1m
Plastic carpet	< 1.25m
Laminate	< 1.25m

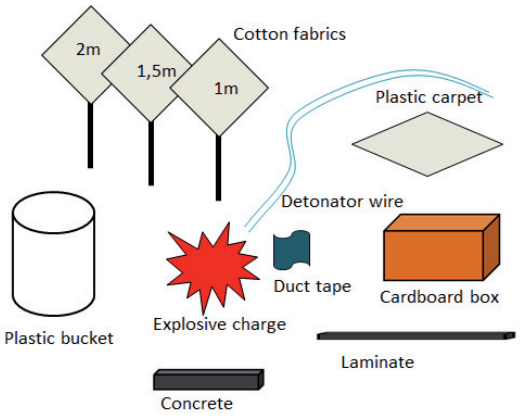

Figure 1. Left: Distances between targets and explosive material. Right: Scheme of the test setup.

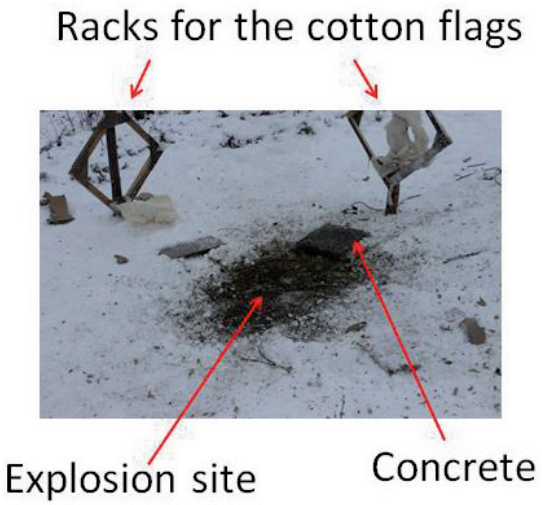

Figure 2. Explosion site after the blast.

The explosions were carried out within one hour at noon in winter conditions with mild wind and frost. There was also a thin snow on the ground. TNT was exploded at first, dynamite as the second and PENO as third. More detailed weather information for the time of each explosion may be seen in Table 1.

Table 1. Weather conditions during the experiment.

	Day	Hour	Min	Temp °C	Humidity %
TNT	22.10.2013	11	20	-2.2	80
Dynamite	22.10.2013	12	20	-2	80
PENO	22.10.2013	12	50	-2	76
	Wind dir.	Wind speed	Wind blasts	Atm. pressure	Visibility
TNT	178	3.6	7	1025.6	50 000
Dynamite	201	2.2	4	1025.5	43 160
PENO	198	1.9	4.7	1025	39 710

After each explosion, remains of the ten sample collectors were gathered and stored by an experienced crime scene investigator by following the approved procedures of forensic inspection. Due to the different kind of explosives and the type of detonation, there was some variation in the size of the remains which were left of the sample collectors. However, as the power of each blast had been defined in advance, pieces could be collected well after each blast. Due to the winter conditions, they were, however, partially covered by snow, and after storing samples in plastic bags the snow melted into water when the bags were brought inside. That may have washed some of the explosion residues away from the samples, but despite of that positive results of the residues were found in some samples with all of the analyzing methods which were used in the study.

When a high energetic material reacts, it can detonate, deflagrate or do the both. The rate of the detonation or deflagration has a major influence on the remaining traces. Detonation is chemically an oxidation reaction which does not involve external oxygen. In the explosion the detonation material involves chemically unstable molecular structures or functional groups that can split into gaseous products and heat (with supersonic reaction speed). Deflagration for its part is a thermal process that proceeds radially outwards away from the ignition source in all directions through the available material. Deflagration can also be incomplete, in which case the reaction can generate various number of different decomposition products.[5]

The physical state of the energetic material has an effect on the proceeding reaction type. For example, using a dense plastic explosive, a shock wave proceeds with the detonation. If the explosive has a granular form, the shock wave of the detonation can terminate and continue as an incomplete deflagration. In this experiment, PENO and dynamite were detonated while granular TNT was deflagrated. As a result of the deflagration, TNT residues were found well on most of the sample materials in the ATR FTIR analysis and quite well also in VNIR, SWIR and MWIR hyperspectral analysis. However, traces of dynamite and PENO were not reliably found in ATR FTIR nor in hyperspecral analysis, which may be explained by their complete explosions, easily evaporated EGDN and high performance compared to TNT.[4]

2.2 ATR FTIR spectroscopy

The ATR FTIR technique is commonly used by military and forensic investigators and by traveling and transportation security officials at the airports. Extensive libraries and advanced device technologies have allowed the wide use of IR- techniques. For example the HazMat FTIR-series is a good example of mobile IR-devices on the market. However, additional basic research is required for the identification of new compounds on complex sample matrixes.[6–9]

In this study IR screening was used for testing this analyzing method on explosives per se, and as a comparative technology for the hyperspectral analysis on the same samples. The preparations of the samples were kept simple. The ATR FTIR-analysis was carried out directly on the explosive materials and on the post-blast

residues. Measurements were made directly on the solid samples and on dried rinse samples on an aluminum foil.

The measurements were made on pure explosives of TNT, dynamite and PENO, and on nine of the ten residue collectors which were used in the tests. Residues on laminate were not measured because of the size of the sample, and because of the melting snow on it. IR spectroscopy results are thereby available from cotton fabric at three distances from the explosive charge, plastic bucket, cardboard box, detonator wire, concrete, duct tape and plastic carpet.

The IR measurements were measured with a Bruker ATR platinum Diamond spectrometer by using the basic measurement mode (range 4000 – 400 cm^{-1}; resolution 4 cm^{-1} and 32 scans). Identification of the explosive materials was carried out by comparing the measured spectra of the pure explosive materials on the cotton fabric with the post-blast residue samples. The absorbance to transmittance-converting and baseline correction of the measured spectra were processed by OPUS 7.0-software.[10]

The ATR FTIR-spectra of the pure explosives were measured by soaking the explosive materials on a clean cotton fabric at first, and by measuring the spectrum of the explosive on the cotton after that. The influence of the background material was reduced of the measurement results after the measures, so the samples represent concentrated wiping samples of the pure explosives used in the test.

The IR analysis of the post-blast residue samples was made in two ways. The residues were at first measured directly on the collected pieces without any sample preparation or wiping in between. After that, rinsed samples of the collected pieces were produced with acetone. Solid samples were rinsed by using 5 ml of acetone, and then filtered (Whatman 40) and evaporated on an aluminum foil. When the dilutions were evaporated completely, IR-spectrum was measured on the aluminum foil.

2.3 Hyperspectral imaging and analysis

The detetction, separation and identification of explosives and explosive residues with hyperspectral analysis was the primary purpose of this study. For veryfying hyperspectral test results, same samples were analysed also with the IR spectroscopy.

Three different types of hyperspectral imagers were utilized and compared for screening efficacy during the study. Spectral range of the devices reached from visible light to mid-wave infrared. Imagers were manufactured by Specim Ltd. Technical details of the imagers are found in the Table 2.

Table 2. Technical properties of the hyperspectral camera equipment used in the study.

material	VNIR	SWIR	MWIR
Spectral Range	400 - 1000 nm	970 - 2500 nm	2000 - 6000 nm
Number of spectral bands	96	256	256
Spectral resolution	2.8 nm	10 nm	35 nm
Number of pixels/image line	1000	320	320

The detection of explosive residues was performed in two phases. First, the spectra of the explosive substances were detected from the samples of pure explosives. After that the target detection algorithm was used for finding the residues of pure substances from the pieces of various materials which had been collected from the explosion site. Test targets were also classified with a spectral classification algorithm for combining the results. False color images of the pure samples imaged with each hyperspectral camera are presented in Figure 3. As Figure 3 reveals one can see from the VNIR data that the pure TNT and Dynamite are clearly visually distinguishable, but the difference between them is not as clear. The false color images of the SWIR and MWIR data suggest that the explosives may have some characteristic features at those wavelengths.

The extraction of the spectra for the explosives was made by using vertex component analysis (VCA).[11] VCA is a widely utilized computationally efficient way to induct endmembers from spectral data. The basic

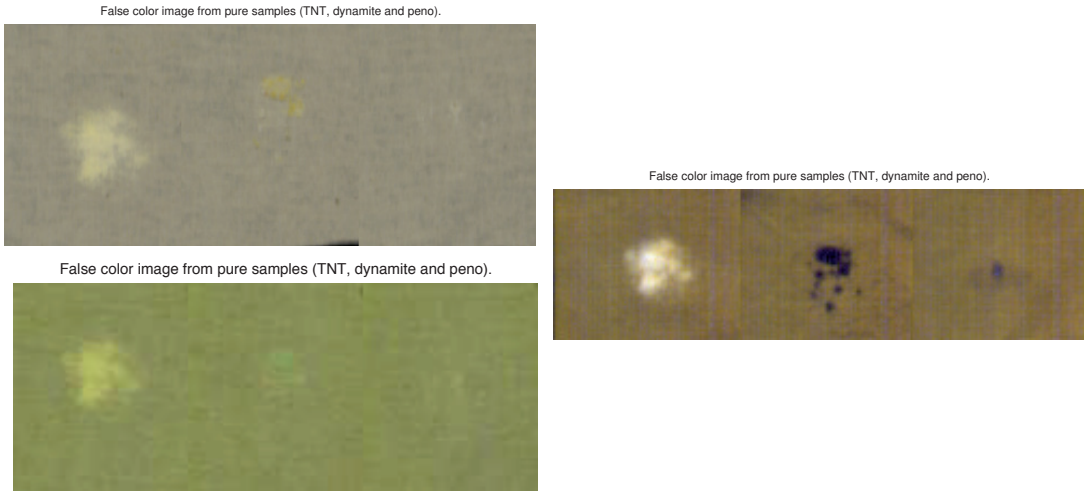

Figure 3. False color images with narrow wavebands showing pure explosives on the piece of cotton fabric. In each image there is a small amount of TNT, dynamite and PENO (from left to right). Top-left: VNIR, Bottom-left: SWIR and Right: MWIR.

idea behind VCA is to orthogonally project spectral data to a lower dimensional space and to detect there an extremeity vertex of the convex hull covering the data points. In the case of the VCA it is a pre-requisite to know how many endmembers the algorithm is intended to generate. The endmember induction process is sensitive to this setting, because it continues from one projection and extremity vertex to next until it reaches the number of endmembers required. Additionally, in VCA the spectral data is assumed to be a linear mixture of endmembers.

In this experiment, VCA was performed separately for each camera's data. As a result endmembers were received for each data set. These spectra are illustrated in Figure 4. Discovered endmembers can be verified by calculating the inversion back to the original spectral data. In this case computationally costly non-negative constraint least squares (NNLS)[12] were used on each pixel of the test samples to determine the abundance images for each inducted endmember.

There is reason to assume that the post-blast explosive residues are more or less subpixel-scale in data. This means that also a subpixel level method is needed for finding these small particles. In this case, a small combination of algorithms, including VCA and NNLS as their core components, was utilized for this purpose. In the the HFC method[13] which was applied in this analysis, the virtual dimension number will be calculated first in order to determine the potential number of endmembers in the data. After that the VCA will be utilized to extract the endmembers. Then the target endmember signature will be added to the results from the VCA step. If the VCA finds an endmember which is very similar to the target endmember, this matching endmember will be displaced by the original target endmember. The comparison is performed with a spectral angle mapper (SAM)[14] algorithm. It measures the spectral similarity by finding the angle (in radians) between endmember $\mathbf{e} = (e_1, e_2, \dots e_L)^T$ and imaged spectrum $\mathbf{s} = (s_1, s_2, \dots s_L)^T$ so that,

$$sam = \cos^{-1}\left(\frac{\sum_{l=1}^{L} e_l s_l}{(\sum_{l=1}^{L}(e_l)^2)^{1/2}(\sum_{l=1}^{L}(s_l)^2)^{1/2}}\right),$$

where L is number of wavebands in spectra. SAM is meant for the signature vector based target discrimination and identification. It gives values for each pixel in the image and is computationally cheap. If the degree of mixing between the imaged spectra is low, SAM should work efficiently, but because in this case we are looking for subpixel traces, SAM will not give very accurate results.

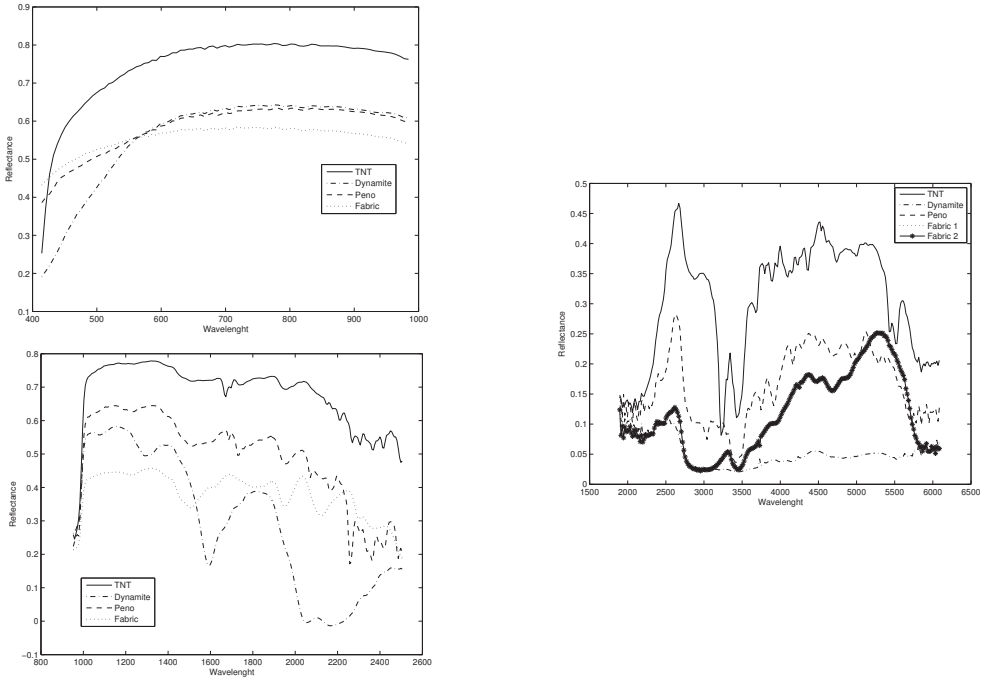

Figure 4. Endmembers extracted from each imager's data with VCA. Top-left: VNIR, Bottom-left: SWIR and Right: MWIR.

After determining the endmember set the NNLS is calculated. As an output the algorithm provides the abundance data for the target endmember. Figure 5 shows these abundance maps for the pure explosive substances. Basically endmembers for TNT and dynamite can be detected in data from all of the three cameras. PENO is distinguishable only with SWIR and MWIR cameras.

3. RESULTS AND DISCUSSION

3.1 ATR FTIR-spectroscopy of the pure explosive materials and post-blast residues

The processed IR-spectra of the wiping samples the tested pure explosive materials are presented in Figure 6. Explosive materials in all of these samples contain -ONO2 or -NO2 groups which are recognized in the IR-spectrum. The main component of the Fordyn-dynamite is AN, which is shown in the same region as the pure AN in its own spectrum. The main differences between TNT, dynamite and PENO are the aromaticity of TNT the molecule, type -NO2 group and the distribution of the components.[15] A characteristic peak of the DMDNB is shown in the fingerprint region of the PENO-spectrum, even if the intensities of the peaks are weak as a result of 1 % concentrate.

The IR-spectra of the post-blast residue samples were compared with the absorbance spectra of the pure explosive materials which were generated to the library of the OPUS-software. The identification was accomplished by using direct-methods.

The post-blast residue samples were measured directly from the samples without any preparations, and from rinsed samples which were produced with acetone. The solid samples were rinsed from the background material with a minimum volume of acetone, which was then filtered and evaporated on the aluminum foil. When the dilutions were evaporated until dry, IR-spectrum was measured on the aluminum foil.

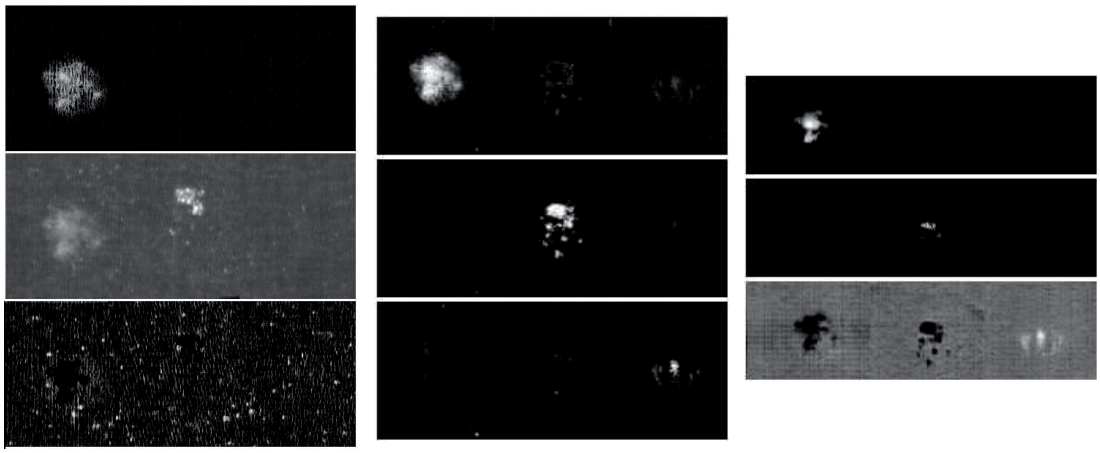

Figure 5. Target detection abundance maps for each imager, VNIR (left), SWIR (middle) and MWIR (right). Top map in each column represents TNT, dynamite in the middle and PENO below. As can be seen below on the left, the endmember for PENO was not found with the VNIR imager. In the SWIR and MWIR data all of the three substances are found.

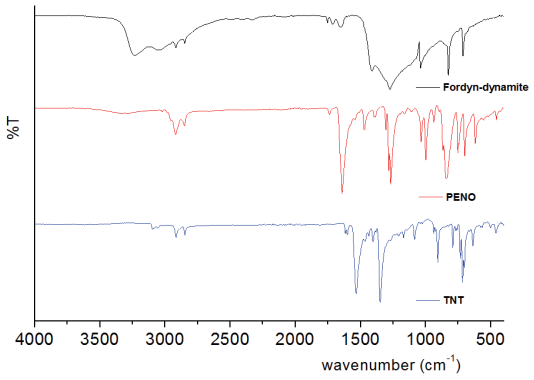

Figure 6. IR-spectrum of the pure explosive materials.

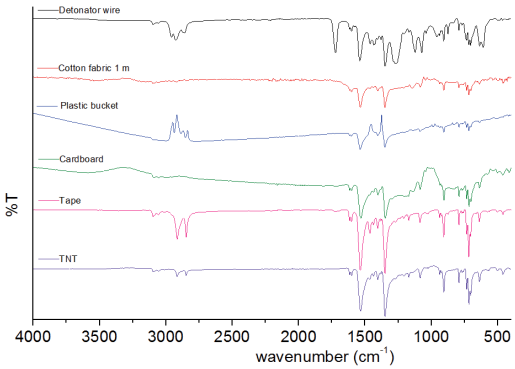

Figure 7. IR-spectrum of the post-blast residue samples, measured directly on the materials without any sample preparation. Identification by the OPUS-software.

Sample / target material	Directly on the material	Rinsed sample
Cotton flag (50*50cm) 1m	+	+
Cotton flag (50*50cm) 1.5m	–	+
Cotton flag (50*50cm) 2m	–	+
Plastic bucket	+	+
Cardboard box	+	+
Detonator wire	+	
Wiping sample (concrete)	–	+
Plastic tape	+	–
Plastic carpet	–	–

+ positive identification; – negative identification

Figure 8. Outline of the TNT sample identification by ATR FTIR

The IR-spectra of the TNT post-blast residue samples, which were measured directly on the materials collected from the explosion site, are presented in Figure 7. The spectra contain almost all peaks of the pure TNT. There are also some additional peaks in some of the materials because of the missing of the background reduction. Nevertheless, all crucial peaks are shown for the identification of the TNT in the post-blast residue samples.

The rinsed samples were produced with an easily evaporating acetone, which is an inert and appropriate solvent for the TNT residues. The aluminum foil was found to be a suitable zero background material for the evaporation and for the measurements of the rinsed and dried samples. In the measurements the rinsed samples were utilized as concentrated wiping samples.

The spectra of the rinsed samples were clearer than the spectra which were measured directly on the objects which were collected from the explosion site. Positive results for TNT were found in all sample materials except on the plastic carpet. The moisture of some of the samples (created by the melted snow) made the search of the explosion residues more difficult, which can explain the missing positive result in some of the measures. An outline of the detection of TNT residues on direct and rinsed samples is illustrated in Figure 8.

3.2 Hyperspectral analysis results

Shortly after the explosion tests the collected sample materials were imaged with three hyperspectral cameras. After the measurements data analysis was carried out as is described in section 2.3. As can be seen in Figures 5 and 9, the SWIR data gives the clearest result for the detection of pure explosive residues.

Using the target detection algorithm gives with some of the samples reasonably clear results. For example in Figure 10 can be found some subpixels, which are identified to contain traces of TNT. However, there are also some false indications, like in the analyzing results of the duct tape and some plastic samples. In these cases

Figure 9. False color image of abundance of pure substances

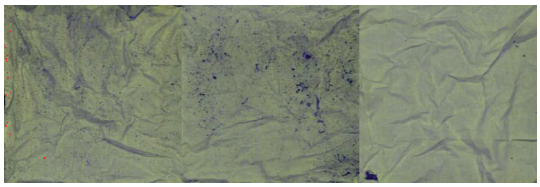

Figure 10. The detection of TNT residues from the cotton fabric. Three fabrics were placed at a different range from the explosive charge (100, 150 and 200 cm; in image from left to right). Traces of TNT were found with all of the three hyperspectral cameras on a fabric which was placed at 100 cm from the charge.

the same algorithm gave indications of dynamite from a sample which was taken from the explosion with TNT. (There is, however, a small chance that the sample contains dynamite, or that the algorithm gives a positive result for dynamite instead of TNT because of the similarities in the chemical structure of these substances.)

It is also possible to use SAM to give some insight on the accuracy of the method. As can be seen in Figure 11, SAM classifies each explosive correctly with pure materials. On the left in Figure 11 are classification results for SWIR data and on the right for MWIR data (TNT = red, Dynamite = blue, PENO = yellow). In Table 3 are represented the minimum values of SAM for each target material and for each camera. As was mentioned earlier, an endmember for PENO could not be extracted from VNIR camera data. If the results for pure explosives and explosive residues are compared, it seems that the minimum SAM for explosive residues is many times higher than for pure substances. Thus, based on this information it is not clear that the correct indications concerning the presence of explosive residues can be confirmed with SAM.

4. CONCLUSION

The objective of this study was to test whether the selected explosives can be detected, identified and separated as pure substances and explosive residues with an IR spectrometer and with three different hyperspectral cameras with the wavelengths of VNIR, SWIR and MWIR areas. The experiment was made as controlled explosions at winter time outdoor conditions, after which the wiping samples of pure explosives and explosion residues on several different test materials were analysed with the ATR FTIR spectrometer and with three different hyperspectral cameras. The analysis with the IR spectrometer included direct measurements on the samples and measurements on the dilluted samples. All hyperspectral analyses were made on data which was measured

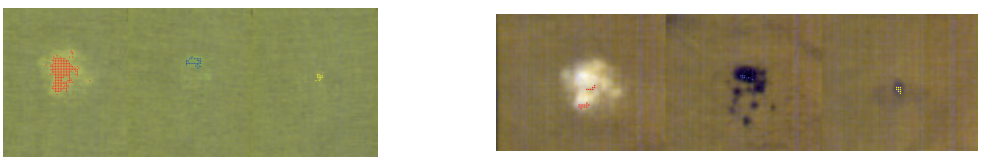

Figure 11. On the left are SAM classification results for SWIR data and on the right for MWIR data (TNT = red, Dynamite = blue, PENO = yellow)

Table 3. Smallest found spectral angle between targets and detected endmembers for explosive materials.

Explosive material	Spectral imager	Pure Sample	Cotton fabric	Plastic bucket	Duct tape
TNT	VNIR	0.006	0.019	0.024	0.025
	SWIR	0.011	0.105	0.063	0.041
	MWIR	0.036	0.135	0.208	0.162
Dynamite	VNIR	0.006	0.031	0.037	0.036
	SWIR	0.057	0.295	0.325	0.347
	MWIR	0.201	0.172	0.285	0.188
PENO	VNIR	n/a	n/a	n/a	n/a
	SWIR	0.022	0.122	0.095	n/a
	MWIR	0.075	0.134	0.172	n/a

directly on pure explosive substances and on objects (residue collectors) which were collected on the explosion site after each blast.

The results show that the spectra of the pure substances of the tested three explosives, TNT, dynamite and PENO, can be detected and separated both with the ATR FTIR spectrometer, and with all of the three tested hyperpectral cameras, VNIR, SWIR and MWIR. Also the post-blast explosive residues of TNT were detected on cotton fabric with all of these four technologies. With the ATR FTIR spectrometer post-blast residues of TNT were also found on plastic bucket, cardboard box, detonator wire, concrete (wiping sample) and on duct tape. Also the hyperspectral cameras found some sparate traces of TNT, for example the VNIR camera on the cotton fabric at three different range from the explosive charge, and SWIR camera on the duct tape. However, post-blast traces of dynamite and PENO were not detected with any of the four IR technologies, which may at one part be explained by the detonation type of explosion of dynamite and PENO, and by the deflagration of TNT.

Table 4. Comparison of TNT results between hyperspectral imaging and ATR FTIR measurements. (+ = found, - = not found)

Target		ATR FTIR	VNIR	SWIR	MWIR
Cotton fabric	100 cm	+	+	+	+
	150 cm	-	+	-	-
	200 cm	-	+	-	-
Plastic bucket		+	-	-	-
Duct tape		+	-	+	-

If the direct measuring results of the explosion residues of TNT are compared between hyperspectral imaging and ATR FTIR spectrometry, one can observe in Table 4 that there might be some correlation between ATR FTIR, SWIR and MWIR results, especially with traces on cotton. From this one can conclude that it might be possible to detect some post-blast explosive residues through the use of hyperspectral imaging. However, further research and experiments are needed for making more confimed conclusions on this topic. As the size of the measurement area is different in ATR FTIR and hyperspectral imaging, in the research ATR FTIR measurements should be taken precisely on the same spot on the target materials as where the hyperspectral imaging is being done. Closer examination may be focused on spots where positive results have been received with either of the technology. In the hyperspectral analysis, it also seems that the HFC is affected by noisy data, so it should be

replaced with a less noise sensitive method.

ACKNOWLEDGMENTS

This research has been funded by Tekes - the Finnish Funding Agency for Innovation and by the University of Jyväskylä.

REFERENCES

[1] Gallagher, E. M., [*Molecular Analysis of Active Degraders and metabolic*] (2010).

[2] Republic, C. and Republic, S., "Some experience with trace analysis of post- explosion residues," *AARMS* **3**(4), 633–646 (2004).

[3] Song-Im, N., "Explosive residue analysis : Evaluation and optimisation of sampling," *Storage and Cleanup Protocols* , 1–212 (2011).

[4] Forcit, L., "Forcit defence." www.forcit.fi/en/forcit-defence-2 (2013).

[5] Akhavan, J. E., [*The Chemistry of Explosives, 2nd ed.*], RSC Paperbacks (2004).

[6] Mou, Y. and Rabalais, J. W., "Detection and identification of explosive particles in fingerprints using attenuated total reflection-fourier transform infrared spectromicroscopy," *J.Forensic Sci.* **54**(4), 846–850 (2009).

[7] Primera-Pedrozo, O. M., Y. M. Soto-Feliciano, L. C. P.-L., and Hernandez-Rivera, S. P., "Detection of high explosives using reflection absorption infrared spectroscopy with fiber coupled grazing angle probe/ftir," *Sens. Imaging* **10**(1-2), 1–13 (2009).

[8] Pacheco-Londono, L. C., Castro-Suarez, J. R., and Hernandez-Rivera, S. P., "Detection of nitroaromatic and peroxide explosives in air using infrared spectroscopy: Qcl and ftir," *Adv. Opt. Tech.* , 1–8 (2013).

[9] Furstenberg, R., Kendziora, C. A., Stepnowski, J., Stepnowski, S. V., Rake, M., Papantonakis, M. R., Nguyen, V., Hubler, G. K., and McGill, R. A., "Stand-off detection of trace explosives via resonant infrared photothermal imaging," *Appl. Phys. Lett.* **93**(22), 224103 (2008).

[10] Bruker, [*OPUS, Spectroscopic Software, Reference Manual*], Bruker, 5 ed.

[11] Nascimento, J. and Dias, J., "Vertex component analysis: A fast algorithm to unmix hyperspectral data," *IEEE Transactions on Geoscience and Remote Sensing* **34**(4), 898–910 (2005).

[12] Bro, R. and De Jong, S., "A fast non-negativity-constrained least squares algorithm," *Journal of Chemometrics* **11**(5), 393–401 (1997).

[13] Chang, C., [*Hyperspectral Imaging: Techniques for Spectral Detection and Classification*], Kluwer Academic/Plenum (2003).

[14] Schowengerdt, R. A., [*Remote Sensing, Third Edition: Models and Methods for Image Processing*], Academic Press, Inc., Orlando, FL, USA (2006).

[15] SDBS, "Spectral database for organic compounds sdbs." http://sdbs.db.aist.go.jp (2013).

PIV

HYPERSPECTRAL IMAGING OF BENTHIC MACROINVERTEBRATES - A NOVEL TOOL FOR DETECTING METAL CONTAMINATION IN RUNNING WATERS

by

Johanna Salmelin, Ilkka Pölönen, **Hannu-Heikki Puupponen**, Heikki Hämäläinen, Anna Karjalainen, Ari Väisänen, Kari-Matti Vuori 2014

Manuscript. To be submitted.

PV

UAV-BASED HYPERSPECTRAL MONITORING OF SMALL FRESHWATER AREA

by

Ilkka Pölönen, **Hannu-Heikki Puupponen**, Eija Honkavaara, Antti Lindfors, Heikki Saari, Lauri Markelin, Teemu Hakala, Kimmo Nurminen 2014

Proc. SPIE 9239, Remote Sensing for Agriculture, Ecosystems, and Hydrology XVI, 923912 (10 October 2014); doi: 10.1117/12.2067422

UAV-based hyperspectral monitoring of small freshwater area

Pölönen I.[a], Puupponen H-H.[a], Honkavaara E.[b], Lindfors A.[c] Saari H. [d], Markelin L.[b], Hakala T.[b] and Nurminen K.[b]

[a]Department of Mathematical Information Technology, University of Jyväskylä, Mattilanniemi 2, 40100 Jyväskylä, Finland;
[b]Finnish Geodetic Institute, Geodeetinrinne 2, 02430 Masala, Kirkkonummi, Finland
[c]Luode Consulting Ltd, Sinimäentie 10 B, 02630 Espoo, Finland
[d]VTT Technical Research Center of Finland, Tietotie 02150, Espoo, Finland

ABSTRACT

Recent developments in compact, lightweight hyperspectral imagers have enabled UAV-based remote sensing with reasonable costs. We used small hyperspectral imager based on Fabry-Perot interferometer for monitoring small freshwater area in southern Finland. In this study we shortly describe the utilized technology and the field studies performed. We explain processing pipeline for gathered spectral data and introduce target detection-based algorithm for estimating levels of algae, aquatic chlorophyll and turbidity in freshwater. Certain challenges we faced are pointed out.

Keywords: Fabry-Perot interferometer, uav, freshwater, target detection, hyperspectral imaging

1. INTRODUCTION

Compact, lightweight hyperspectral imagers have been developed in the recent years, so that they can be utilized also with small sized unmanned aerial vehicles (UAV). Manufacturers such as Cubert, Rikola and Headwall Photonics have been introducing their solutions for spectral imaging from UAV's. Small, light spectral imagers are opening up opportunities to use spectral imaging in new applications. In more traditional spectral imaging applications these small imagers combined with UAV platforms can produce data in circumstances where traditional imagers aren't useful (for example cloudy weather). This combination also provides us with data, which usually has much smaller ground pixels in comparison to traditional spectral remote sensing platforms.

We have been developing and field testing Fabry-Perot interferometer (FPI) based hyperspectral imaging, which Rikola has adopted as a product. In this study we utilized FPI based hyperspectral imaging for monitoring small freshwater area in southern Finland. FPI imager was mounted on a small UAV and several flights were conducted. Our aim was to demonstrate data processing and analysis pipeline for FPI camera. We faced several challenges, which are shortly discussed in this paper. In section 2 we describe imaging system, test measurements, data processing and analysis for FPI based hyperspectral data. In section 3 and 4 we present some analysis results and mainly discuss problems and challenges that arose during the study.

2. METHODS

2.1 Hyperspectral imager

In our study we have been using Fabry-Perot interferometer based hyperspectral imager such as descriped in.[1] Used FPI imager is prototype of Rikola's FPI imager. Imager has been used in several studies for example concerning precision agriculture.[2–4]

The basic principle of this sensor is based on multiple orders of the Fabry-Perot Interferometer (FPI) that are used matched to the different sensitivities of the image sensor channels. When FPI's air gap range is selected correctly, there will be one to three spectral transmissivity peaks, which are recorded with a normal RGB color image sensor. Detector utilized in this study is a CMV4000 4.2 Megapixel CMOS image sensor from CMOSIS.

Further author information: (Send correspondence to Dr. Ilkka Pölönen)
Ilkka Pölönen: E-mail: ilkka.polonen@jyu.fi, Telephone: +358 400 248 140

After capturing image, the spectral information can be retrieved from the Bayer color filter pattern of RGB sensor.

The FPI spectral imager can operate in wavelength range 400 - 950 nm. Although whole spectral area cannot be utilized at once. With long and short pass filters it is possible to select spectral range from 400 to 500 nm, which was used in this study. FPI-based imager is relatively lightweight at only about 600g. In airborne missions data is gathered to a 32 gigabyte compact flash memory card. It is possible to attach irradiance sensor and separate GPS receiver to the instrument. The image resolution in the typical configuration is 1024 x 648 pixels. One major characteristics in use of FPI imager is that different spectral planes of the hyperspectral data cube are collected with small time delays in between. This affects data so that, if FPI camera is in motion, the spectral planes are not perfectly overlapping. Process to align layers is explained in several papers.[4,5] Technical details of FPI imager is presented in Table 1 and in more detail in publications of VTT Technical Research Centre of Finland[1]

Table 1. Specifications of the used hyperspectral imager

Parameter	Specified value	Remarks
Horizontal FOV Vertical FOV	> 50 > 37	
Spectral range	500 900 nm	Spectral range can be selected from range 400 500 nm with long and short pass filters
Spectral resolution	10 - 40 nm, FWHM	The spectral resolution depends on the transmission order of the FPI and on the selected wavelength. For a high spectral resolution the spectral range needs to be limited
Spectral step	< 1 nm	
F-number	2.7	
Image sensor	CMV4000	CMOSIS CMOS image sensor with 5.5 μm x 5.5 μm pixels. Sensor size 2048 x 2048 pixels
Image sensor pixel clock frequency	80 Megapixels/s	Readout of the whole 4 Megapixel image takes 50 ms
Default spectral image dimensions	1024 x 648 pixels	2x binning
Max spectral image dimensions	2048 x 1240 pixels	
Power consumption	< 5W	
Weight	< 600g	
Main dimensions	80 mm x 97 mm x 159 mm	

2.2 Test area and UAV flight campaign

The area of interest is a shallow lake Petäjärvi, approximately of size of 1 km^2, located in the area of the well-known photogrammetric test field Sjökulla in Southern Finland (60 14' 31" N, 24 23' 03" E). The lake consists of two basins having different characteristics (Figure 1).

Several UAV flights were carried out under partially cloudy weather conditions in August 16, 2012. Flights were carried out separately in these two basins due to legislative and technical reasons; two flights in the eastern basin and three flights in the western basin. The FPI camera was operated from a helicopter UAV having a maximum payload of 5 kg (Fig. 1). We used a flying altitude of 150 m, which is the maximum allowed altitude for UAV flights in free airspace in Finland. The resulting GSD was 15 cm and the image footprint was 154 m by 97 m. The spectral camera was operated with many different filter configurations: 400-500 nm, 500-900 nm and

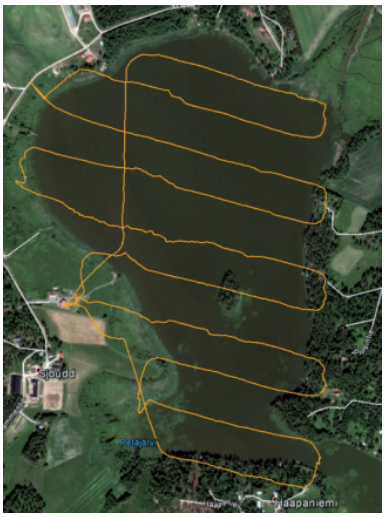

Figure 1. a) The FPI spectral camera in a helicopter UAV. b) UAV flight route over western basin of Petäjärvi

600-750 nm in separate flights; numbers of spectral bands varied between 29 and 42 depending on filters. More details of the campaign are given by Honkavaara et al.[5]

In this investigation we used data from the western basin of the lake collected using 400-500 nm filter configuration. Details of the spectral settings are given in Table 2.

During the campaign, Luode Oy carried out reference water quality measurements with Xylem YSI EXO, which is multisensor system for water quality monitoring. Sensor gathered information about water temperature (average 20.2 C), specific conductance (75.4 $\mu S/cm$), Turbidity (20.4 NTU), chlorophyll a (30.5 $\mu g/L$) and distribution of Blue-Green Algae (14510 cells/ml). Reference information was collected with small boat and saved together with GPS information.

For the radiometric reference we had portable reflectance reference targets. We carried out insitu reflectance measurements using the Avantes hand held spectrometer.

Table 2. Imaging parameters

Area 2, Filter: 400-500 nm, Exposure: 25 ms, 34 layers, Images 0-366, Time: 16.08.2012 15:10:32 to 15:31:08 (UTC +3).
Wavelength (nm): 414.80, 416.20, 416.80, 418.70, 420.50, 422.50, 424.40, 426.40, 428.40, 430.30, 432.20, 434.30, 436.50, 438.50, 440.60, 442.70, 445.00, 447.10, 449.20, 451.20, 474.70, 477.20, 480.00, 482.20, 485.90, 487.50, 488.20, 488.90, 489.20, 489.30, 489.30, 489.60, 489.60, 489.70.
FWHM (nm): 14.22, 14.81, 14.73, 15.62, 15.12, 14.11, 14.37, 14.38, 14.01, 14.43, 14.07, 14.53, 14.42, 14.40, 14.50, 14.84, 14.83, 14.66, 14.67, 14.39, 15.17, 15.56, 14.70, 14.37, 13.34, 12.31, 12.50, 13.49, 13.69, 11.41, 13.87, 11.60, 12.10, 12.01.

2.3 Data processing

The data processing approach for the FPI imagery has been developed by Mäkynen et al.,[6] Honkavaara et al.,[4] Hakala et al.,[7] and Markelin et al.[8] The phases of the processing were as follows: 1. System corrections of the images using the laboratory calibration, spectral correction and dark signal correction. 2. Matching of layers to form spectral data cubes of individual images. 3. Determination of image orientations of reference layers using a

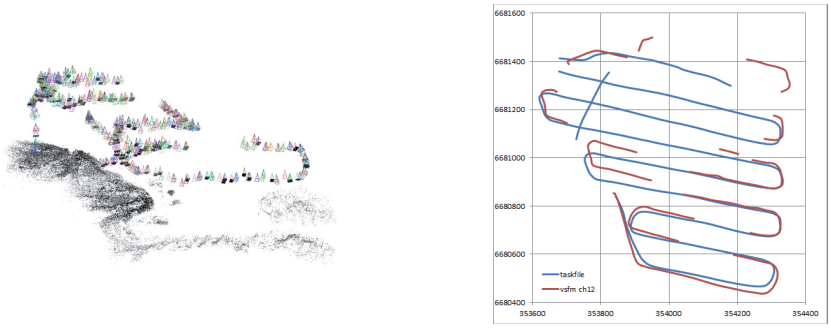

Figure 2. a) Sparse point cloud and perspective centres generated by VisualSFM for a part of the flight. b) GPS-traectory and trajectory based on orientation processing by VisualSFM.

self-calibrating bundle block adjustment. The approximate orientations were based on the GPS trajectory data from the UAV and the timing information of images. The VIsualSFM method was used to provide the image rotation information and to enhance the approximate orientations. 4. Determination of radiometric imaging model to compensate atmospheric and illumination influences, and view/illumination related nonuniformity, as well as reflectance transformation. 5. Calculation of spectrometric image mosaics.

In the previous studies the data were collected of vegetated and nonvegetated land surfaces. Some challenges appeared for the proposed method when using it for geometric and radiometric processing of water image data.

Orientation of images consisting exclusively of homogeneous water was challenging, because the orientation method used was based on image matching and in the water images there were not any details suitable for matching. For the same reason, the matching of separate layers of data cubes was not possible in these images. An example of the result of VisualSFM processing indicated that the automated matching of the images with some details such as shoreline or algae or other vegetation in water was successful. The graph in Figure 2 shows where the successful matchings were; there were also gaps in the GPS-trajectory.

We approached the problem so that the orientations of missing images were taken from the flight trajectory determined by photogrammetric block adjustment, utilizing the timing information of individual images. For the band matching we used affine transformation based on the estimated flight speed information. This approach provided slightly lower accuracy than the normal process, but the accuracy was considered to be sufficient for the application with an geolocation accuracy requirement of 10 m.

With the FPI camera, a large number of data cubes (hundreds or more) is mosaicked together in order to create a spectral mosaic over the area of interest. Many disturbances influence the digital numbers; these have to be compensated for in order to create reflectance values characterizing the object. In our campaigns, the most important correction factors were the radiometric calibration of the camera and the correction for view/illumination-direction effects (bidirectional reflectance distribution function; BRDF). Our approach was first to apply the laboratory calibration corrections to the images, and then, to calculate empirical radiometric BRDF correction. Finally, the radiometrically corrected DNs were transformed to reflectance by using the reflectance targets. The details of the method are described by Honkavaara et al.[5]

The radiometric quality of the spectral mosaics was quite poor if we did not perform any radiometric corrections (Fig. 3 a). We tested the existing procedure[5] but it did not provide sufficient quality. Possible explanations for this were that the BRDF model used was not suitable for the data and that there were remaining inaccuracies in the sensor calibration. We estimated a calibration image using homogeneous water images to eliminate potential errors in the sensor calibration; this improved the quality, but not enough. We also used BRDF correction for the recalibrated images, which improved the results further (Fig. 3 c). Finally, we estimated a flight line dependent calibration image (Fig. 3 d); this approach appeared to provide the best results. In principle, this correction eliminates impacts of both of the error sources stated above. Some remaining errors are still visible in Fig. 3 d. One possible explanation could be that the yellow-blocking filter used in front of the optics that

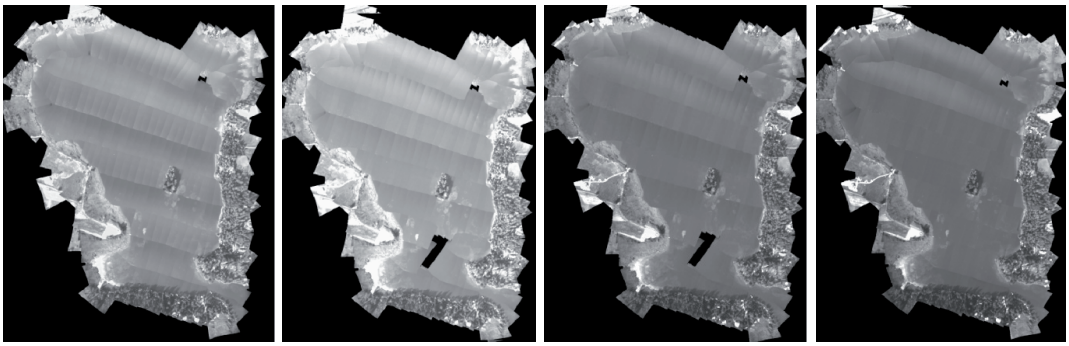

Figure 3. Mosaics of band 15 provided of the data. From left: (a) not any radiometric corrections, (b) using calibration image based on median image, (c) using calibration image based on median image calculated for each flight direction and (d) b with BRDF correction.

was not included in calibration caused some additional lens falloff effects that could not be eliminated with the available correction methods. Another possible explanation could be incompletely corrected BRDF effects, and the sun glint, which occurs in imagery when the water surface orientation is such that the sun is directly reflected towards the sensor.

2.4 Target detection system

Our assumption was that levels of turbidity, green-blue algae and chlorophyll could be estimated as a linear mixture of their and freshwater's reflectance spectra. Turbidity was thought to be correlating with spectrum of soil. These spectra were extracted from literature.[9,10] In Figure 4 there are shown the chosen reflectance spectra for these substances. These spectra could thus be used as spectral endmembers. Endmembers are characteristic spectra for certain substances.

If $\mathbf{y}$ is detected spectra and $\mathbf{x_i}$ represents endmembers, then linear mixture model is

$$\mathbf{y} = \sum_i a_i \mathbf{x_i},$$

where a_i is relative abundance of each endmember in detected spectrum. Now we can calculate inversion to solve linear equation. Or we could calculate abundance of each selected spectra with target detection algorithm. Both methods would give us subpixel level information about distribution of different values.

Our inversion is based on fast non-negative least squares solution (FNNLS).[11] Target detection algorithm uses HFC method,[12] vertex component analysis,[13] spectral angle mapper (SAM)[14] and FNNLS. First HFC is used to calculate virtual dimension number. Based on this number of endmembers is estimated from data. Then VCA is used to extract that many endmembers. VCA projects data orthogonally to lower dimensional space using principal components analysis. In projected space data points can be covered by a convex hull. The vertices of this hull are potential endmembers of spectral dataset. VCA tries to find these vertices. The number of supposed endmembers affects this process greatly, because VCA continues from one projection and extremity vertex to next until it reaches required number of endmembers.

After that each extracted endmember is compared with set of target spectra. Comparison is done using spectral angle mapper. It measures spectral similarity by finding the angle (in radians) between endmember $\mathbf{e} = (e_1, e_2, \dots e_L)^T$ and imaged spectrum $\mathbf{s} = (s_1, s_2, \dots s_L)^T$ so that,

$$sam = \cos^{-1}\left(\frac{\sum_{l=1}^{L} e_l s_l}{(\sum_{l=1}^{L}(e_l)^2)^{1/2}(\sum_{l=1}^{L}(s_l)^2)^{1/2}}\right),$$

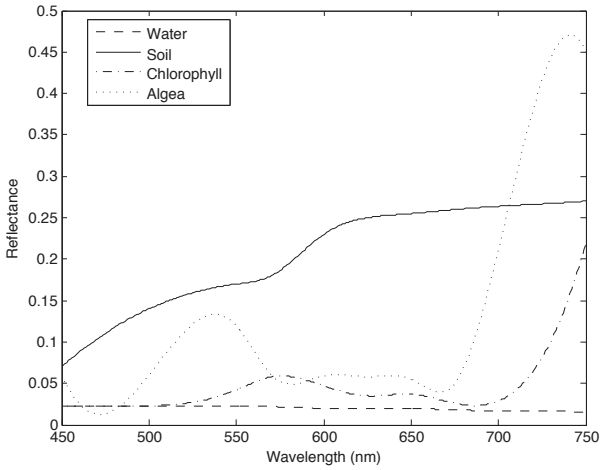

Figure 4. Reflectance spectra for water, soil, green-blue algae and chlorophyll.

where L is number of wavebands in spectra. If spectra are sufficiently similar then endmember is replaced with target. Otherwise target is added to group of endmembers. After detection of endmembers FNNLS is calculated and abundance of target in data is determined. Figure 5 illustrates outline of the target detection process.

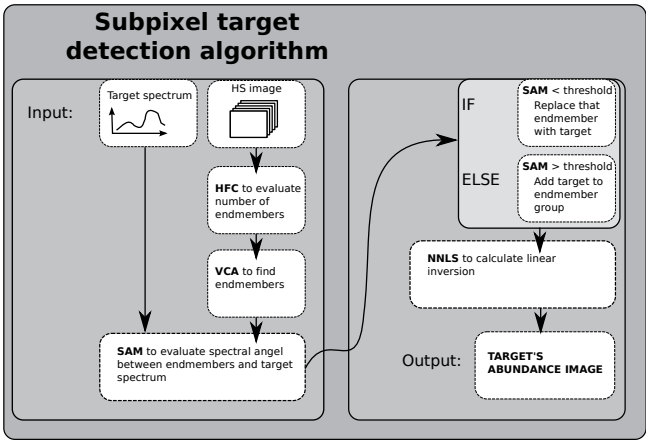

Figure 5. Outline of target detection algorithm.

3. RESULTS

As Figures 2 shows, we managed to process separate hyperspectral cubes to one image mosaic. Also radiometric corrections were performed. Visual presentation of different analysis methods is presented in Figure 6. First column of images shows results of target detection algorithm, second column presents results of linear inversion based on the library spectra and last column is spectral angle mapper calculations for the lake. As images show, abundance of targets/endmembers are almost non-existent in lake surface area proper. This has influence to correlation between target/endmember abundance and reference water quality measurements.

Correlation coefficients between these images and measured reference values varied between 0 and 0.25. None of the calculated features had good correlation between samples. There are several reasons why this may have happened. First, Petäjärvi is a small and quite dark lake surrounded by farms. This affects water quality so that turbidity is high. This means that signal achieved from water is low in intensity. It is possible that signal to noise ratio is also so low that little variations on signal disappear into the noise. Secondly, if we look at Figure 4 our target spectra have characteristic features starting from 500 nm. They are quite similar to each other between 400-500 nm. Thirdly, it may be that assumption of a linear mixture is incorrect or it isn't good enough approximation for these spectra. It is also possible that reflectance spectra gathered from library have been biased.

4. CONCLUSION AND DISCUSSION

We used a novel FPI spectral camera to provide spectral mosaics of a small inland lake Petäjärvi in Finland. The camera is tuneable based on separate spectral filters and a Fabry-Perot interferometer. Our investigation focused on developing suitable processing methods for the new kind of spectral data. We also tested the potential of narrow spectral bands for monitoring turbidity using 13 spectral bands in 400-500 nm region. The results indicated that the method was suitable for the water monitoring. We expect that improving the direct measurements of sensor orientation and irradiance information will make the processing more robust and automatic.

We present two different methods how to estimate level of algae, aquatic chlorophyll and turbidity in water. Although previous section shows, that we couldn't achieve good results compared to measured reference water quality values. We have also images covering wavelengths 500 - 900 nm taken with different settings. Due to some schedule issues we didn't have time to as of yet process that data. Combining existing mosaic to non-processed data with wider spectral range, the results of analysis process could have been considerably better and extracted features might potentially have correlated better with reference water quality measurements.

Currently we have ongoing research project concerning water monitoring, in which we have been developing both preprocessing chain for FPI-based hyperspectral imager and analysis methods. We have had freshwater hyperspectral imaging campaigns from manned and unmanned aerial vehicles during the summer 2014. We hope that these observed problems have been avoided in these other campaigns.

It is important to understand that the entire data production chain impacts the radiometric data quality. We will take this into account in the future campaigns. The system calibration will be further emphasized, so that there will not be any uncalibrated phenomenon in the optical path. The BRDF and sun glint impacts can be efficiently eliminated by using larger side overlaps in the image blocks so that the mosaics can be formed using images with small view zenith angles. In some cases the flight paths can be directed so that the BRDF effects are minimized, by flying towards the sun. It is also essential to continue investigation of the empirical radiometric correction methods for small format UAV image blocks collected in challenging imaging conditions.

ACKNOWLEDGMENTS

Study has been partly funded by Finnish Innovation agency Tekes.

REFERENCES

[1] Saari, H., Pölönen, I., Salo, H., Honkavaara, E., Hakala, T., Holmlund, C., Mäkynen, J., Mannila, R., Antila, T., and Akujärvi, A., "Miniaturized hyperspectral imager calibration and uav flight campaigns," *Proc. SPIE* **8889**, 88891O–88891O–12 (2013).

[2] Pölönen, I., Saari, H., Kaivosoja, J., Honkavaara, E., and Pesonen, L., "Hyperspectral imaging based biomass and nitrogen content estimations from light-weight uav," *Proc. SPIE* **8887**, 88870J–88870J–9 (2013).

[3] Kaivosoja, J., Pesonen, L., Kleemola, J., Pölönen, I., Salo, H. A., Honkavaara, E., Saari, H., Mäkynen, J. H., and Rajala, A., "A case study of a precision fertilizer application task generation for wheat based on classified hyperspectral data from uav combined with farm history data," in [*Remote Sensing for Agriculture, Ecosystems, and Hydrology XV*], *Proc. SPIE* **8887** (2013).

[4] Honkavaara, E., Hakala, T., Kirjasniemi, J., Lindfors, A., Mäkynen, J., Nurminen, K., Ruokokoski, P., Saari, H., and Markelin, L., "New light-weight stereosopic spectrometric airborne imaging technology for high-resolution environmental remote sensing case studies in water quality mapping," *ISPRS - International Archives of the Photogrammetry, Remote Sensing and Spatial Information Sciences* **XL-1/W1** (2013).

[5] Honkavaara, E., Saari, H., Kaivosoja, J., Pölönen, I., Hakala, T., Litkey, P., Mäkynen, J., and Pesonen, L., "Processing and assessment of spectrometric, stereoscopic imagery collected using a lightweight uav spectral camera for precision agriculture," *Remote Sensing* **5**(10), 5006–5039 (2013).

[6] Mäkynen, J., Holmlund, C., Saari, H., Ojala, K., and Antila, T., "Unmanned aerial vehicle (uav) operated megapixel spectral camera," in [*Electro-Optical Remote Sensing, Photonic Technologies, and Applications V*], Bishop, G. J., Kamerman, G. W., Gonglewski, J. D., Steinval, O., and Lewis, K. L., eds., *Proc. SPIE* **8186** (2011).

[7] Hakala, T., Honkavaara, E., Saari, H., Mäkynen, J., Kaivosoja, J., Pesonen, L., and Pölönen, I., "Spectral imaging from UAVs under varying illumination conditions," *ISPRS - International Archives of the Photogrammetry, Remote Sensing and Spatial Information Sciences* **XL-1/W2**, 189–194 (2013).

[8] Markelin, L., Honkavaara, E., Näsi, R., Nurminen, K., and Hakala, T., "Geometric processing workflow for vertical and oblique hyperspectral frame images collected using uav," *ISPRS - International Archives of the Photogrammetry, Remote Sensing and Spatial Information Sciences* **XL-3**, 205–210 (2014).

[9] Thenkabail, P., Lyon, J., and Huete, A., [*Hyperspectral Remote Sensing of Vegetation*], CRC Press/Taylor & Francis (2012).

[10] Sridhar, B. M. and Vincent, R. K., "Spectral reflectance measurements of a microcystis bloom in upper klamath lake, oregon," *Journal of Great Lakes Research* **33**(1), 279 – 284 (2007).

[11] Bro, R. and De Jong, S., "A fast non-negativity-constrained least squares algorithm," *Journal of Chemometrics* **11**(5), 393–401 (1997).

[12] Chang, C., [*Hyperspectral Imaging: Techniques for Spectral Detection and Classification*], Kluwer Academic/Plenum (2003).

[13] Nascimento, J. and Dias, J., "Vertex component analysis: A fast algorithm to unmix hyperspectral data," *IEEE Transactions on Geoscience and Remote Sensing* **34**(4), 898–910 (2005).

[14] Schowengerdt, R. A., [*Remote Sensing, Third Edition: Models and Methods for Image Processing*], Academic Press, Inc., Orlando, FL, USA (2006).

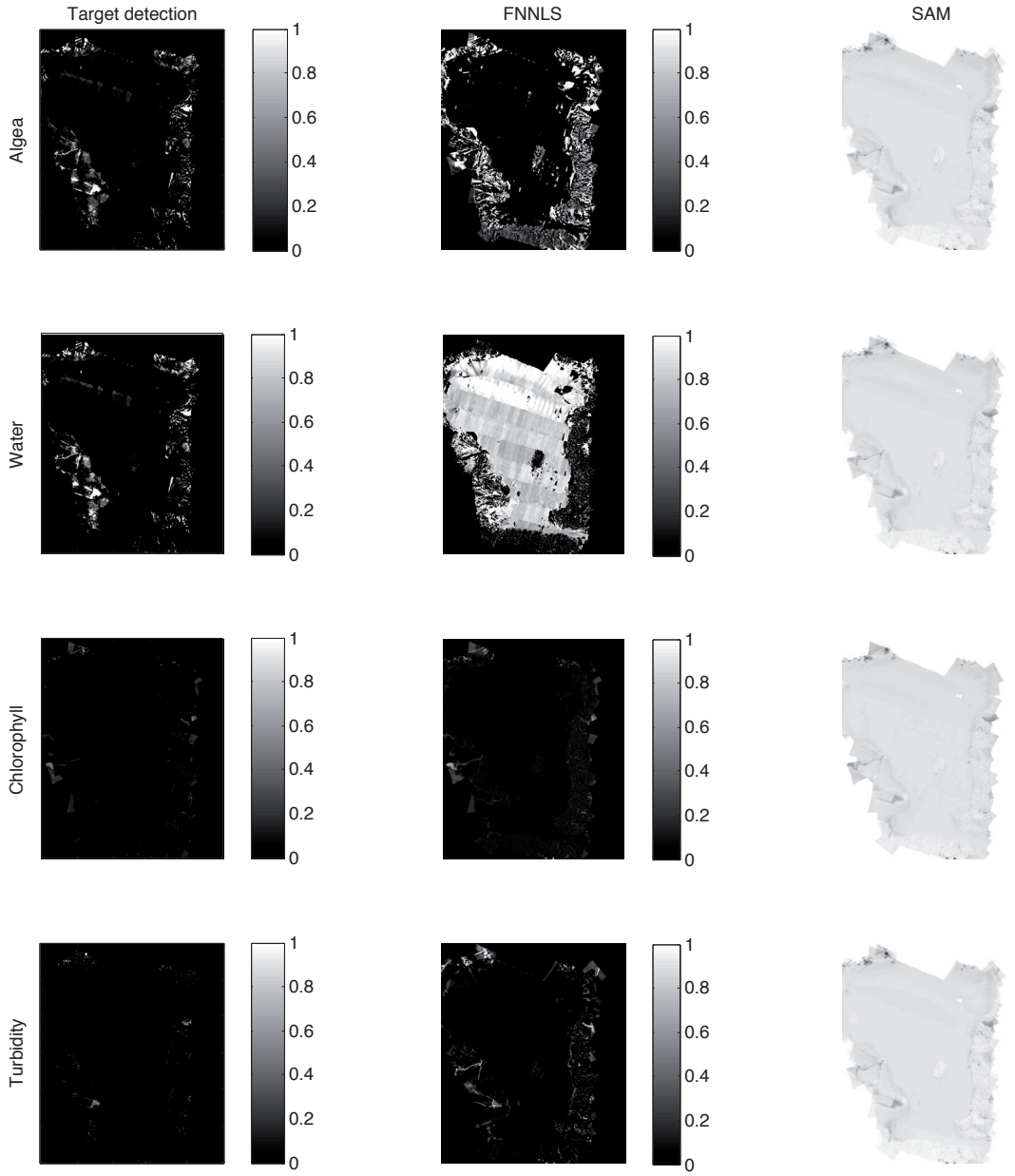

Figure 6. Results from target detection algorithm (1st column), FNNLS (2nd column) and SAM (3rd column). Each row represents different material algea (1st row), freshwater (2nd row), chlorophyll (3rd row) and soil/turbidity (4th row). Target detection algorithm and FNNLS produce relative abundance maps, where values vary from 0 to 1. This means that value 1 is perfect match. SAM represents angle in radians between target spectrum and detected spectrum. In case of SAM value 0 is perfect match.

PVI

SPECTRAL UNMIXING FOR THE SEPARATION OF LENTIGO MALIGNA AND LENTIGO MALIGNA MELANOMA

by

Hannu-Heikki Puupponen, Ilkka Pölönen, Noora Neittaanmäki-Perttu, Pekka Neittaanmäki, Mari Grönroos, Heikki Saari 2014

Submitted to Medical Engineering and Physics, Elsevier